Annu. Rev. Nucl. Part. Sci. 1990. 40: 285–326

PAIRING CORRELATIONS AND TWO-NUCLEON TRANSFER BETWEEN HEAVY NUCLEI

C. Y. Wu

Nuclear Structure Research Laboratory, University of Rochester, Rochester, New York 14627

W. von Oertzen

Hahn-Meitner-Institute, D-1000 Berlin 33, Germany

D. Cline

Nuclear Structure Research Laboratory, University of Rochester, Rochester, New York 14627

M. W. Guidry

Department of Physics, University of Tennessee, Knoxville, Tennessee 37996; and Physics Division, Oak Ridge National Laboratory, Oak Ridge, Tennessee 37831

KEY WORDS: transfer reactions.

CONTENTS

0163–8998/90/1201–0285$02.00

1. INTRODUCTION

The concept of direct transfer of one or more nucleons between colliding nuclei has played a pivotal role in our understanding of shell structure in nuclei. Single-nucleon transfer is a selective and direct probe of single-particle shell structure, while two-nucleon transfer is a direct probe of pairing correlations in nuclei. The reaction dynamics for transfer reactions with light ions is well understood in terms of the distorted-wave Born approximation (DWBA) (1). Thus light-ion-induced one- and two-nucleon transfer reactions have been exploited for almost four decades to study single-particle structure and two-particle correlations in nuclei.

The reaction mechanism for heavy-ion-induced transfer reactions is considerably more complicated because strong inelastic excitation causes the "directness" to be obscured by multistep processes. This complication, coupled with the limited energy resolution attainable in heavy-ion reactions, has slowed progress both theoretically and experimentally for few-nucleon transfer in heavy-ion reactions. Nevertheless, heavy-ion-induced transfer reactions exhibit unique features that have the potential of adding a new dimension to the use of transfer reactions for probing nuclear structure. One feature is that the de Broglie wavelength is small, and the loss of energy and angular momentum during the collision are sufficiently small that the reaction mechanism may be approximated well by semiclassical methods. A second feature is that appreciable Coulomb excitation of the incoming nuclei, prior to transfer, allows study of the transfer of nucleons between excited states. Coulomb excitation selectively populates low-lying collective states. Thus heavy-ion-induced transfer reactions make it possible to study transfer of nucleons between especially interesting collective states in deformed nuclei. In particular, it opens the possibility of studying the evolution of single-particle structure and the modification of pairing with increasing angular momentum. Heavy-ion transfer reactions also provide a unique population mechanism that has many advantages for studying moderate- and high-spin nuclear states in the yrast domain.

The primary motivation of this review is to exploit the specificity of heavy-ion-induced two-nucleon transfer reactions to probe pairing correlations in heavy nuclei (2). One application is to investigate the importance of nonzero spin terms in the pairing potential, that is, the relative

importance of s, d, and g pairs (3). Recent theoretical and experimental (4, 5) studies of two-neutron transfer explore these effects. Of considerable interest is the study of the transition from the superfluid to the normal phase that occurs at high angular momentum when the pairing is quenched by the Coriolis force. An interesting phenomenon is the predicted oscillation in phase of the pair transfer matrix elements as a function of angular velocity in certain deformed nuclei (6). The phases change at certain rotational frequencies and chemical potentials where band crossing occurs. These are called diabolical points, and the phase change can be understood in terms of a general topological phase elucidated by Berry (7).

The study of analogs of solid-state pairing phenomena in nuclei can advance understanding of pairing in both nuclear and solid-state many-body systems. An especially interesting aspect that may be explored with heavy-ion transfer reactions is related to the "superfluidity" of nuclei and the possibility of searching for nuclear analogs of the Josephson effect (8–11). When two superfluid nuclei are brought together in a collision at energies below the Coulomb barrier, the study of multiple pair transfer in a tunneling process is similar to that of a supercurrent passing through the insulating barrier between two superconductors. Large enhancement for pair transfer reactions has been reported quantitatively for the system Sn+Sn (12, 13) and qualitatively for Sn+Dy (13). This is the first step toward identifying the nuclear Josephson effect. Enhancement of multiple pair transfer was also found recently in proton transfer channels (14).

This article describes recent theoretical and experimental developments for studying transfer reactions between heavy nuclei. A general discussion of reaction dynamics and pairing effects in heavy-ion transfer reactions is followed by a description of the recent development of experimental techniques. A discussion of general features of heavy-ion-induced few-nucleon transfer reactions and specific quantitative comparisons are presented in Section 4, which emphasizes the study of the enhancement and the oscillating nature of two-nucleon transfer associated with pairing correlations. The article concludes with a summary of the outlook for further development of the experimental and theoretical techniques, and with the outstanding scientific opportunities they will provide for probing nuclear structure.

2. HEAVY-ION TRANSFER REACTIONS

2.1 *Semiclassical Description of Transfer Reactions*

It is well known that for heavy-ion collisions classical scattering orbits give a very good quantitative description of various processes (15). The relation between the distance of closest approach R_{min} and the center-of-mass

scattering angle θ_{cm}, for a given center-of-mass energy E_{cm} (see Figure 1), is given by

$$R_{min} = \frac{Z_1 Z_2 e^2}{2E_{cm}}\left(1+\frac{1}{\sin\theta_{cm}/2}\right). \quad 1.$$

The reaction cross section is obtained by multiplying the reaction probability by the scattering cross section. Most reactions discussed here are assumed to occur at or below the "Coulomb barrier." This implies that the contribution of the nuclear potential to the Coulomb potential ($\geq$200–300 MeV) can be neglected in the definition of the Rutherford scattering orbit. More relevant to the discussion of the reaction probabilities is the amount of density overlap, which we parametrize by removing the $A^{1/3}$ dependence of projectile and target through the overlap parameter d_o

$$d_o = R_{min}/(A_1^{1/3}+A_2^{1/3}), \quad 2.$$

where A_1 and A_2 are the masses of the two nuclei. This gives a measure of nuclear overlap at closest approach independent of the size of the system. If each reaction angle corresponds to only one R_{min}, which is always the case for energies below or close to the Coulomb barrier, a unique transformation of the θ or E_{cm} into d_o (R_{min}) can be obtained. In addition, we discuss only reactions where $R^i_{min} \approx R^f_{min}$, the scattering orbits are matched so as to obtain sizable cross sections (see the discussion of Equation 5 below). Thus the discussion of the relevant physical quantities measured will not be given as function of (θ, E_{cm}) but rather in terms of d_o. Various processes (absorption, transfer, excitation, etc) have form

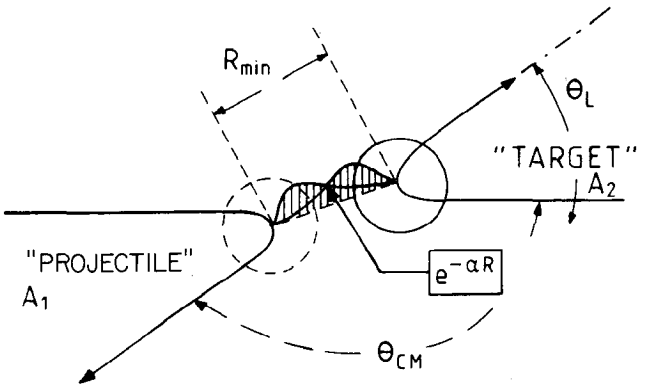

Figure 1 Definition of the reaction angle θ_{cm} and R_{min}, close to the Coulomb barrier, for heavy-ion collisions.

factors that are slowly varying compared with the wavelength of relative motion λ:

$$\lambda = \hbar/\sqrt{2m_{aA}E_{cm}}, \qquad 3.$$

where m_{aA} stands for the reduced mass in the scattering system. Generally, absorption is associated with a large number of channels, in which case it can be described by an imaginary potential or directly by an absorption function, $P_{abs}(d_o)$ or $P_{abs}(\theta)$. The elastic scattering is now written in terms of a Rutherford cross section multiplied by a "survival" function,

$$\frac{d\sigma_e}{d\Omega}(\theta) = \frac{d\sigma_R}{d\Omega}(\theta)[1 - P_{abs}(\theta)]. \qquad 4.$$

The probability of observing elastic scattering is just $(1 - P_{abs})$. Typical data for transfer reactions on ^{120}Sn show a rather universal behavior for the quantity σ_e/σ_R as a function of d_o (Figure 2) (16). Absorption becomes appreciable at an overlap of approximately $d_o \lesssim 1.5$ fm and reaches $\sigma_e/\sigma_R \approx 0.1$ at an overlap parameter of $d_o \approx 1.4$ fm for most systems (16). The fact that the absorption functions are almost universal for heavy systems of different size suggests that nucleon transfer is determined primarily by the geometry and dynamics of the two-center complex formed by the two nuclei.

By definition, absorption in these cases is caused by all interactions that remove flux from the elastic + inelastic channel; these include few-nucleon transfer channels, as well as deeply inelastic and fusion reactions. In an explicit treatment of all nucleon orbits in a two-center potential, nucleons in these events are promoted outside of the configurations close to the Fermi level, which creates exit channels with complete dissipation of probability.

For the description of transfer processes, a factorization of the probabilities P_t and the dynamical factors $F(Q, L)$ connecting the initial and final scattering orbits can be shown to be a good approximation (16, 17). Thus, we have, in first order, the transfer cross section $d\sigma_t/d\Omega$:

$$\frac{d\sigma_t}{d\Omega}(\theta) = \frac{d\sigma_e}{d\Omega}(\theta)P_t(\theta)F(Q, L), \qquad 5.$$

where $P_t(\theta)$ stands for a transfer probability, which describes the transfer at a given separation of the two ions and which we assume can be treated as a perturbation, where $F(Q, L)$ is a dynamical matching factor describing the effects of mismatch of initial and final R_{min} and orbital angular momentum transfer. Generally, $P_t(\theta)$ can be related to the square of the transfer form factor (see Section 2.2) for a first-order process; we call it the transfer

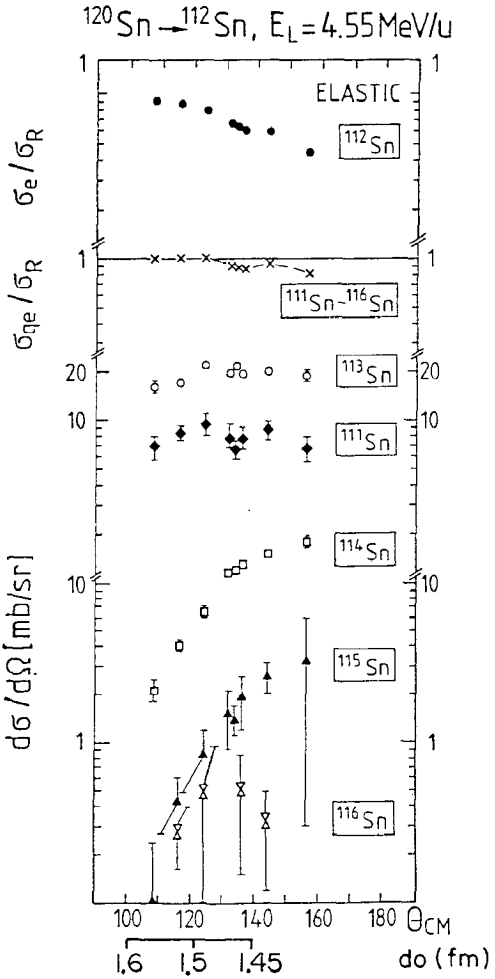

Figure 2 Angular distributions for neutron transfer reactions for ^{120}Sn on ^{112}Sn. The elastic (including inelastic excitation of ^{112}Sn and/or ^{120}Sn) and total quasi-elastic σ_{qe} (elastic+transfer) reactions are also shown. Reproduced from Ref. 12.

function. The same quantity can be defined from calculated values (using DWBA; see next section) of $\sigma_t(\theta)$ and $\sigma_e(\theta)$. For both cases, an exponential parametrization gives a satisfactory description of the asymptotic behavior of the $P_t(d_o)$ function at large separation distances

$$P_t(d_o) = N \exp[-2\alpha d_o(A_1^{1/3} + A_2^{1/3})]. \quad 6.$$

Generally the decay constant α is related to the reduced mass μ_N and

the binding energy E_B of the bound particle. For neutrons we have $\alpha = \sqrt{2\mu_N E_B/\hbar^2}$. For charged particles, an effective binding E_B^{eff} must be used with an exponential (Equation 6), or it can be directly obtained from Equation 5 by fitting the calculated value of σ_t/σ_e (see next section). The probability for multinucleon transfer is obtained, assuming successive transfer, from the product of the probabilities:

$$P_{xn} = P_{1N}^{(1)} P_{1N}^{(2)} \ldots P_{1N}^{(x)} \approx P_{1N}^{x}. \qquad 7.$$

Here P_{1N} stands for the probability of transferring one nucleon. Only in special cases can the individual steps be considered equal. In cold multinucleon transfer, the radial dependence of the transfer function has a steeper slope with increasing number of transferred nucleons; i.e. from Equation 7 we obtain $\alpha_{xn} \approx x\alpha$, as illustrated schematically in Figure 3. Note that the slope of the transfer function for multinucleon transfer is insensitive to whether the transfer occurs in a two-nucleon cluster or in sequence since the pairing energy is small relative to the binding energy.

In order to assess the behavior of individual steps, in particular for proton transfer, explicit DWBA calculations must be performed. The same holds for the dynamical matching factor $F(Q, L)$, which can be obtained from DWBA calculations or expressed in an analytical form using the semiclassical approach (17). The reactions proceed with optimum probability if the initial and final orbits match. In terms of distance of closest approach, the matching condition reads $R_{min}^{i} = R_{min}^{f}$. The turning points are determined by the charge product $Z_1 Z_2$, the center-of-mass energy, and the angular momentum. The optimum Q value (Q_{opt}) for neutron transfer is equal to zero, while for charged-particle transfer $Q_{opt} \neq 0$ it is the deviation ΔQ from the optimum value as well as the angular momentum transfer ΔL (this is also called l later on) that is important for the outcome of the reaction. From the semiclassical theory the factor $F(Q, L)$ is obtained in the form of a Gaussian function depending on ΔQ and ΔL (12, 17),

$$F(Q, L) = \exp[-C_1^2(\Delta Q - C_2 \Delta L)^2], \qquad 8.$$

where ΔQ is given by

$$\Delta Q = Q - Q_{opt} = Q - \left(\frac{Z_c}{Z_A} - \frac{Z_c}{Z_b}\right) E_B + \left(\frac{m_c}{m_b} - \frac{m_c}{m_A}\right)(E - E_B), \qquad 9.$$

for the process $a + A \rightarrow b + B$ with $a = b + c$ (c refers to the transferred particle), while C_1 is a measure of the reaction time,

$$C_1 \approx \left[\frac{r_B m_{aA}(1/\alpha)}{4(2E - E_b)\hbar^2}\right]^{1/2}, \qquad 10.$$

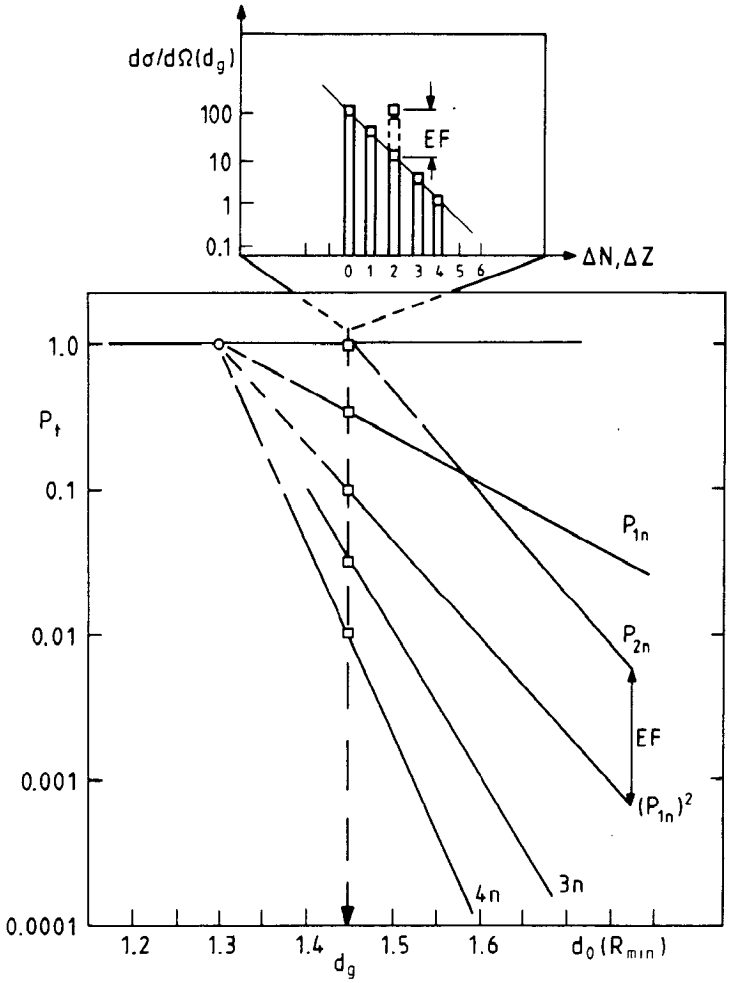

Figure 3 Schematic graph of transfer functions for one- up to four-neutron transfer. Enhancement of P_{2n} relative to P_{1n}^2 is indicated by factor *EF*. The insert shows the expected yield of isotopes on a logarithmic scale.

which depends on the asymptotic slope of the transfer form factor α and on the acceleration at the turning point, which in turn depends on the relative energy available $(E-E_B)$. The coefficient C_2 is a measure of the change of the centrifugal potential that leads to a corresponding change in R_{min}. It is given by

$$C_2 \approx \frac{\hbar^2(L+1/2)}{m_{aA}R_{min}^2}. \qquad 11.$$

For heavy systems and low relative angular momenta L, the contribution of the C_2 term to the width of the Q dependence is small.

In the discussion of the experimental results, the dynamical matching factor plays an important role; therefore we give in Figure 4 two examples for the factor $F(Q, L)$, which were calculated using the computer program Ptolemy (18). Results obtained from experimental systematics, where the whole low-lying excitation energy spectrum is summed, and which represent the dynamical sum-rule limit for single-particle strength, are discussed in Section 4.

In most cases it is necessary to calculate the Q-value and l-value (which is identical to ΔL used earlier) dependence of the cross section using quantal approaches (DWBA; see next section) or to use measured systematics (19) for the final discussion of the transfer functions.

2.2 *The DWBA Description of Two-Nucleon Transfer*

Methods to calculate nucleon transfer by a perturbative approach in terms of DWBA have been discussed extensively during the past 20 years (1). There has been much work on those features that are more specific to reactions induced by heavy ions. Whereas for single-nucleon transfer quantitative agreement with data is generally obtained, it has been extremely difficult to attain quantitative agreement, either in the shapes of angular distributions or in the absolute magnitude for two-nucleon transfer cross sections. Two relevant aspects contribute significantly to this difficulty: (*a*) the possibility of having both one-step pair transfer and sequential transfer; and (*b*) the role of configuration mixing and the question of the inclusion of higher shells.

It is sufficient to make one-step calculations with cluster-wave functions for the evaluation of the quantitative features of the dynamical factors. The differential cross section is given by the expression

$$\frac{d\sigma}{d\Omega}(\theta) = \frac{k_f}{k_i}\sum_{lm} |T_{lm}(\theta)|^2. \qquad 12.$$

The reaction amplitude T_{lm}, characterized by an angular momentum transfer l (and its projection m), can be calculated by most finite-range DWBA computer programs (18). It is given by the six-dimensional integral,

$$T_{lm} = \int \chi_f^*(r_f k_f) \langle \Psi_B^* \Psi_b^* | V_{eff} | \Psi_A \Psi_a \rangle \chi_i(r_i k_i)\, dr_f\, dr_i. \qquad 13.$$

Here the distorted waves $\chi_{f,i}$ are obtained by fits to the elastic scattering as defined previously. The multipolarity (l, m) of the internal matrix element is

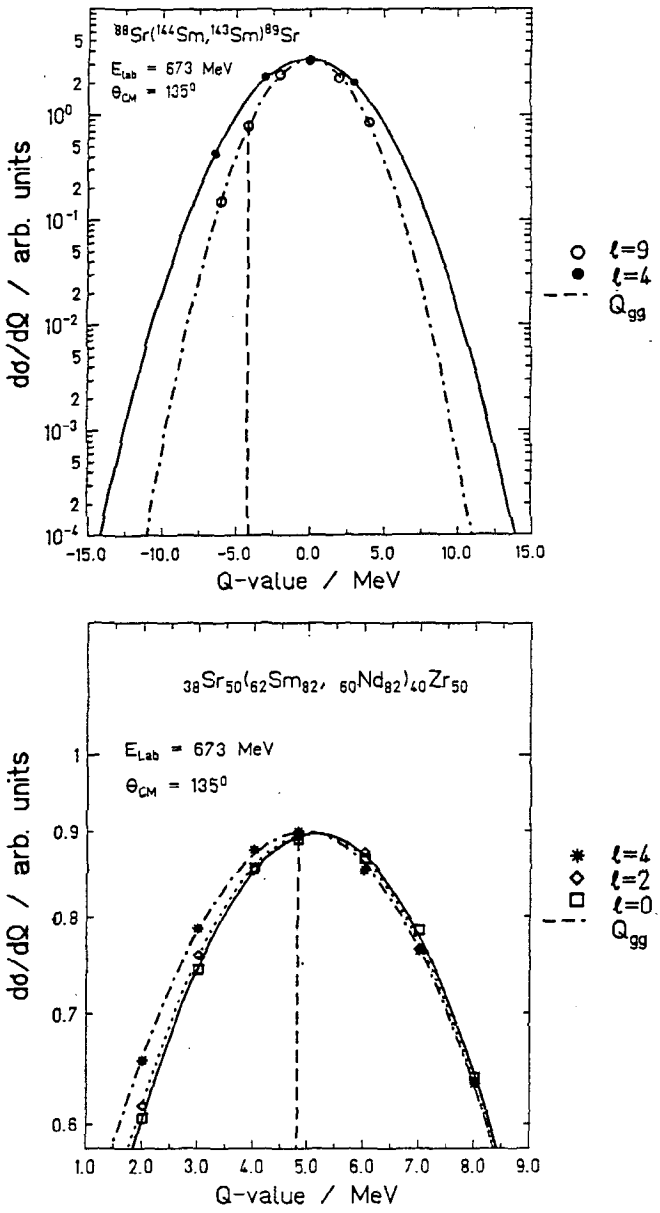

Figure 4 Calculated Q dependence of the differential cross section for one-neutron transfer (*top*) and two-proton transfer (*bottom*); calculated points and a fit by a Gaussian are shown. The *dashed line* shows the ground-state Q value.

obtained with the usual angular momentum coupling rules between the bound states defined by the overlap of the intrinsic nuclear wave functions:

$$\langle \Psi_B | \Psi_A \rangle = N_f \Phi_{l_f}(r_{x_f}) \quad \text{and} \quad \langle \Psi_b | \Psi_a \rangle = N_i \Phi_{l_i}(r_{x_i}). \qquad 14.$$

For large values of r_{x_i}, r_{x_f}, the functions Φ_{l_i}, Φ_{l_f} can be approximated by exponentials fitted to Hankel or Whittaker functions. The intrinsic matrix element in Equation 13 corresponds to the transfer function $P_t^{1/2}(r)$, which has been introduced within the semiclassical approach. As already mentioned, its asymptotic behavior at large separation distances can be approximated by an exponential function. Calculations for one- and two-neutron transfer in the case of $^{112}Sn + ^{120}Sn$ show the expected exponential behavior at large separation distances with a slope parameter α that is, within 10%, given by the value calculated with the simple expression $e^{-2\alpha R}$ introduced in the previous section.

2.3 *Sequential (Two-Step) and One-Step Two-Nucleon Transfer*

The DWBA amplitude through second order for two-particle transfer separates into three pieces (10, 11, 20, 21):

$$T_{2N} = T_{\text{Seq}}^{(2)} + T_{\text{NO}}^{(2)} + T_{\text{Sim}}^{(1)}, \qquad 15.$$

a second-order purely successive term $T_{\text{Seq}}^{(2)}$, a second-order "non-orthogonality" term $T_{\text{NO}}^{(2)}$, and a first-order simultaneous transfer term $T_{\text{Sim}}^{(1)}$. In the limit $V_{12} = 0$, corresponding to pure shell-model wave functions with no residual correlation, the nonorthogonality term $T_{\text{NO}}^{(2)}$ exactly cancels the first-order term: $T_{\text{NO}}^{(2)} = -T_{\text{Sim}}^{(1)}$. In this limit the DWBA reaction proceeds sequentially, and the two-nucleon transfer amplitude is a sum of products of two first-order single-nucleon transfer amplitudes. This result is used in the semiclassical approach for the discussion of enhancement (Section 2.4).

The other limit, where the interaction V_{12} is large (strong correlation limit), corresponds to strongly mixed two-nucleon wave functions. If this mixing is coherent, such that the amplitudes add with similar phases, both the one-step and two-step transfer may be strongly enhanced. If the configuration space is expanded to many major shells, the one-step cross section is found to increase and to converge in realistic cases, whereas the sequential processes will eventually be cancelled by contributions of opposite sign from alternating shells.

In nuclei sufficiently removed from closed shells, two identical nucleons may be coupled to a spin-zero Cooper pair by the short-range residual interaction V_{12}. The strength of this coupling may be measured by the

energy gap $2\Delta \approx 2$ MeV required to break a pair. On the other hand, the individual nucleons are bound to the nuclear mean fields by energies of order 10 MeV. Thus, even in strongly paired systems the pairing correlations are only a perturbation on the independent particle motion, and it is not surprising that sequential transfer is found to play a dominant role in microscopic DWBA calculations (10, 11, 20, 21).

This does not mean that a cluster approximation for transfer cannot be used effectively in heavy-ion transfer. For example, the primary effect of including only one-step DWBA processes for two-nucleon transfer is to scale the total cross section by some constant (often large) amount. However, these results imply that the clusters entering heavy-ion multiparticle transfer are highly effective clusters, operated on by an effective transfer interaction. An important theoretical question to be addressed for the reactions discussed here is whether or not such effective transfer interactions can be determined reliably.

2.4 *Enhancement of Two-Nucleon Transfer*

The concept of enhancement is essential to the discussion of the transfer of Cooper pairs because it is a quantitative measure for the collectivity of the transition, and the relation to the pure single-particle limit is important for the microscopic understanding of the transfer process. The dynamical features of the pairing phase are connected to the fluctuation in particle (pair) number (2). The pairing vibration, as a precursor of the phase transition to the superfluid case (pairing rotations), will show some enhancement (analogous to the quadrupole vibrations of spherical nuclei) in two-particle transfer; the transitions between members of a pairing rotational band should be strongly enhanced and of equal strength within a sequence of nuclei.

Similar to the case of Coulomb excitation of deformed rotational bands, the collective enhancement of a dynamical transition may be expressed in appropriate single-particle units. In pairing vibrations and rotations, the enhancement has been extensively discussed for (t, p) reactions by Broglia, Hansen & Riedel (2). For the pairing rotations, the one-step pair transfer is given in terms of the pairing interaction parameters G (strength) and Δ (gap parameter) by $d\sigma(\text{p.r.})/d\Omega \approx (2\Delta/G)^2$, but the cross section for a single-particle configuration is proportional to $(j+1/2)$. Thus the net result for the enhancement (2) in the tin isotopes is ~ 100 (with $\Delta = 1$ MeV, $G = 0.1$ MeV, and average j value $= 7/2$).

Calculations based on well-established knowledge of the wave functions for pair transfer involving two tin nuclei for energies near and below the Coulomb barrier have been performed by both Weiss (11), and Broglia et al (10). In these calculations the reaction amplitude for transfer between

two normal states is compared with the superfluid-superfluid case; in both calculations an enhancement factor of between 100 and 1000 is obtained.

We can also introduce a more empirical definition of enhancement based on semiclassical properties of the reaction between very heavy nuclei, where the possible sequential character of the transfer process is invoked. According to Equation 7 the probability for two-nucleon transfer would be given by

$$P_{2N} = P_{1N}^2 \widetilde{EF}. \qquad 16.$$

Here the idealized case is considered first: P_{2N} refers to a $0^+ \rightarrow 0^+$ transition between ground states and P_{1N} refers to a particular single-nucleon transfer. We use the corresponding definition for an overall enhancement, EF, for a situation in which the total probabilities for one- and two-nucleon transfer are measured experimentally. In the logarithmic plot of the transfer functions versus d_o the completely sequential transfer process yields a fan of straight lines (asymptotically crossing the $P_t = 1$ line at the same point if all steps occur with equal probability) with increasing slopes $\alpha_{xn} = x\alpha$, as illustrated in Figure 3. Enhanced transfer will be renormalized by the factor EF. In an experiment on one-nucleon transfer, the sum of single-particle transitions up to a few MeV in excitation energy has been measured with a magnetic spectrometer for $^{112}\mathrm{Sn} + {}^{120}\mathrm{Sn}$, where one transition typically may give 1/20 of the total strength based on the comparison between DWBA calculations and the measured total cross section (12). A similar result is also obtained experimentally with the γ-ray technique (see Section 3.3) if transfer on an odd-mass target is measured, where the final states are partially resolved (13). Similarly the P_{2N} strength, measured with the magnetic spectrometer, may contain three low-lying states (the 0^+, 2^+, and 3^- states) within an excitation energy of a few MeV. The true enhancement $\widetilde{EF}$, to be compared with the microscopic calculations cited above, in this case would be a factor of 400/3 larger:

$$\widetilde{EF} = \frac{P_{2N} \cdot 1/3}{(P_{1N} \cdot 1/20)^2} = EF \cdot 133. \qquad 17.$$

The overall enhancement EF observed in the experiments is generally 3–10, implying the true enhancement $\widetilde{EF}$ is $\approx$400–1300. For sequential transfer, enhancements of this size can be attributed to the coherent action of interference terms.

2.5 *Some Aspects of Transfer on Deformed Nuclei*

Pairing correlations in nuclei, as modified by the deformation and by rotation, can be probed directly by two-nucleon transfer reactions involv-

ing heavy deformed nuclei. In the following, we cite two examples showing interesting interference effects associated with nuclear deformation and the consequence for pair transfer between collective states.

Nuclear deformation increases the number of pairs coupled to nonzero angular momentum relative to that of s pairs (3). Therefore, one expects an increase in the importance of the transfer of d pairs, g pairs, and high-λ pairs in transfer reactions involving deformed nuclei. A recent calculation, within the framework of the macroscopic model for pair transfer and the scaled sudden approximation for rotational excitation, showed distinct features resulting from nonzero spin coupling (4). Figure 5 shows cross sections calculated for the reaction ^{162}Dy(^{116}Sn, ^{118}Sn)^{160}Dy. The reduction of cross section with the addition of d and g pairs is clearly visible for almost every state and is particularly pronounced for the low-spin states. The most unique signature is the oscillating structure for low-

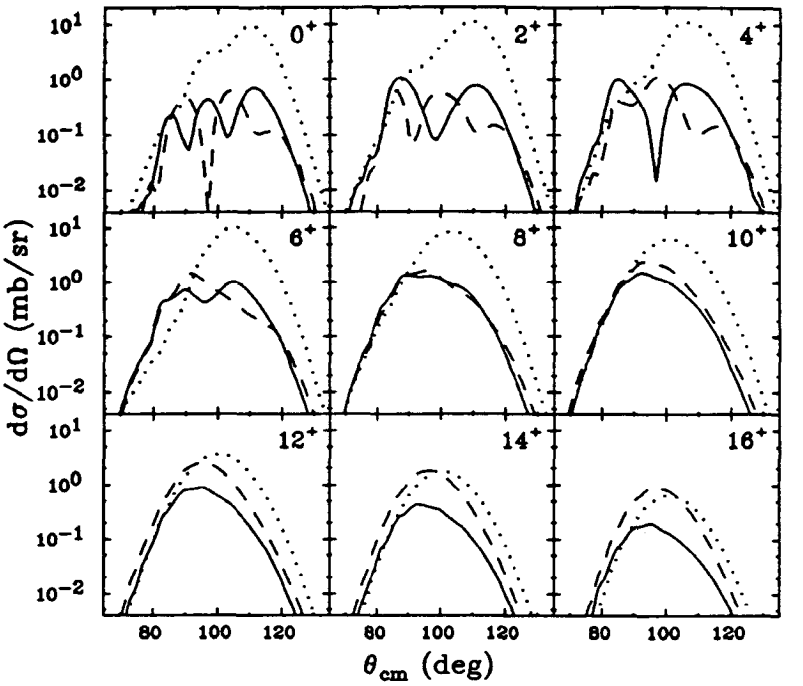

Figure 5 Calculated differential cross sections as a function of the maximum angular momentum carried by the transferred pair (λ_{max}) for the reaction ^{162}Dy(^{116}Sn,^{118}Sn) at E_{lab} = 637 MeV. The *dotted*, *dashed*, and *solid curves* are for λ_{max} = 0, 2, and 4, respectively. Reproduced from Ref. 4.

spin states. Note that this structure in the cross section is also related to the interference between transfers occurring for different orientations of deformed nuclei that classically lead to the same spin (44). Recent experimental evidence (5) for this oscillating structure is discussed in Section 4.1.3.

Another interesting phenomenon is related to diabolic pair transfer in rotating nuclei (6), which is a consequence of a phase change in the pair transfer matrix elements at certain rotation frequencies, called diabolical points. These are connected to a sharp level crossing between the ground-state band and a two-quasi-particle aligned band in deformed nuclei at a certain spin value. Because of strong inelastic excitation, the spin distribution for deformed nuclei, prior to transfer at the distance of closest approach, may overlap with this region of diabolic pair transfer. Thus there is the possibility that the two-nucleon transfer reaction will reflect the destructive interference associated with the Berry phase at the diabolic point (6).

Early calculations (22) of transfer for the reaction of $^{160}Dy + ^{208}Pb$ found no drastic influence of the Berry phase on the two-neutron transfer channel unless the diabolic point, predicted to occur in ^{160}Dy (23), is set artificially low. However, a recent calculation that does not use the scaled sudden approximation for calculating the inelastic excitation, and which includes both an angular-dependent surface form factor plus transfer of pairs coupled with nonzero angular momentum, shows a measurable effect in the populations for states above spin 14^+ (Figure 6) (24). A similar conclusion was reached by de Boer et al (25). Experiments are now searching for this quantum effect involving the Berry topological phase in rotating nuclei (26).

3. EXPERIMENTAL TECHNIQUES

3.1 *Specific Limitations for Heavy Nuclei*

Direct nucleon-transfer reactions measure the overlap of the wave functions of the initial and final states. Interpretation of the data is considerably simplified if the individual final states populated are resolved experimentally. There are two basic methods for resolving the individual final-state population. The first uses thin targets and a high-resolution detection system, such as a magnetic spectrometer, to identify the residual nuclei and resolve the final states. The second method relies on high-resolution studies of the deexcitation γ rays in coincidence with the reaction products for identifying the residual nuclei and deducing the final-state population distribution.

The experimental study of transfer reactions becomes considerably more

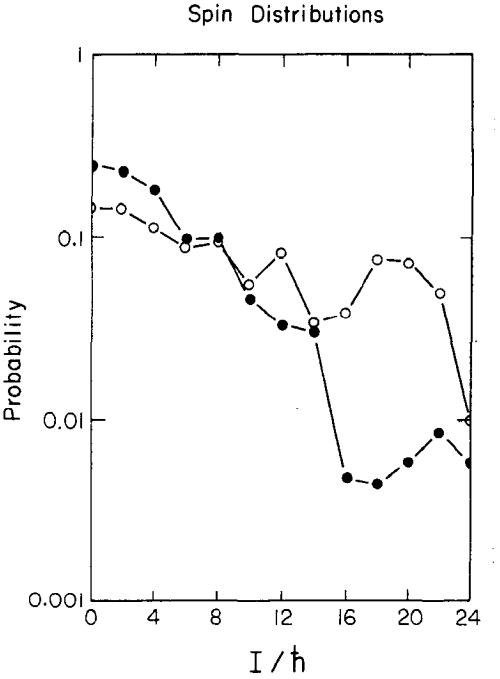

Figure 6 Calculated rotational transfer population patterns for a case with a diabolical point, ^{208}Pb on ^{160}Dy (*filled circles*), and a case without one, ^{208}Pb on ^{158}Dy (*open circles*). The calculation was carried out at $E_{lab} = 1100$ MeV and $\theta = 180°$. The sums of the population probabilities are in both cases normalized to one. (From Ref. 24.)

complicated as the mass of the probing nuclei is increased. Excitation of both residual nuclei becomes important, which exacerbates the problem of resolving final states. The transfer reaction mechanism is complicated by strong inelastic excitation, and also by the increasing importance of non-quasi-elastic channels such as the deep-inelastic and fusion channels as the energy is increased above the Coulomb barrier. To avoid complications associated with the reaction mechanism, it is common to study heavy-ion transfer reactions below or near the Coulomb barrier, where the quasi-elastic channels dominate. This means that the measurements involve backscattering in the center of mass. The kinematics of similar-mass colliding nuclei complicates detection and identification of the backscattered nucleus, even in the favorable case of inverse kinematics. Energy straggling in the target and detector material and the finite energy spread of the incident heavy-ion beams both degrade the energy resolution for heavy-ion reactions.

Transfer reaction measurements at energies below the Coulomb barrier

can be complicated by inelastic scattering or transfer reactions on target contaminants that lead to the residual nucleus of interest. These processes, as well as neutron evaporation channels, can mimic the desired transfer reaction if the target-like residual nuclei are used for identification. This difficulty can be overcome by identifying the isotopically pure projectile-like final nucleus or, better still, by identifying both reaction products.

3.2 *High-Resolution Charged-Particle Detection*

The magnetic spectrometer has for several decades played a key role in the study of light-ion-induced transfer reactions; this work laid the foundation for the theoretical understanding of the direct reaction mechanism, as well as elucidating the importance of shell structure in nuclei. Many of the advantages of the magnetic spectrometer apply equally well to heavy-ion-induced reactions. The development of new focal-plane heavy-ion detectors (27) and the adoption of "inverse" kinematics (12, 14) to detect the more energetic recoiling target nuclei, instead of the backscattered projectile-like nuclei, have facilitated the use of magnetic spectrometers in studies of heavy-ion reactions. As illustrated in Figure 7, unit mass identification up to mass 100 has been achieved (12). An energy resolution of ~ 1.5 MeV has been achieved (28), as illustrated in Figure 8; consequently most individual final states are unresolved, and this technique only observes the gross properties averaged over many final states.

The recoil mass spectrometer (29) provides an elegant solution to the particle identification problem for $A > 100$ and has been used to study heavy-ion-induced transfer (30, 31). Unfortunately, it also suffers from inadequate energy resolution and there is difficulty in ascertaining its absolute detection efficiency.

High-resolution magnetic or recoil mass spectrometers in conjunction with other detectors to identify both reaction products can select unambiguously the reaction channel of interest even when it is only a small fraction of the total quasi-elastic cross section. This approach has the potential of extending the study of sub-Coulomb transfer reactions to lower bombarding energies.

3.3 *Detection of Deexcitation γ Rays*

The inability of charged-particle detection to resolve individual final states is a considerable disadvantage. The resolution of individual final states has proven to be essential for studying interesting phenomena such as the two-neutron transfer between ground states of Sn nuclei or the oscillating structure in the population of the ground band of deformed nuclei populated in two-neutron transfer reactions. Currently the only viable way of resolving the final states of deformed heavy nuclei is through high-resolu-

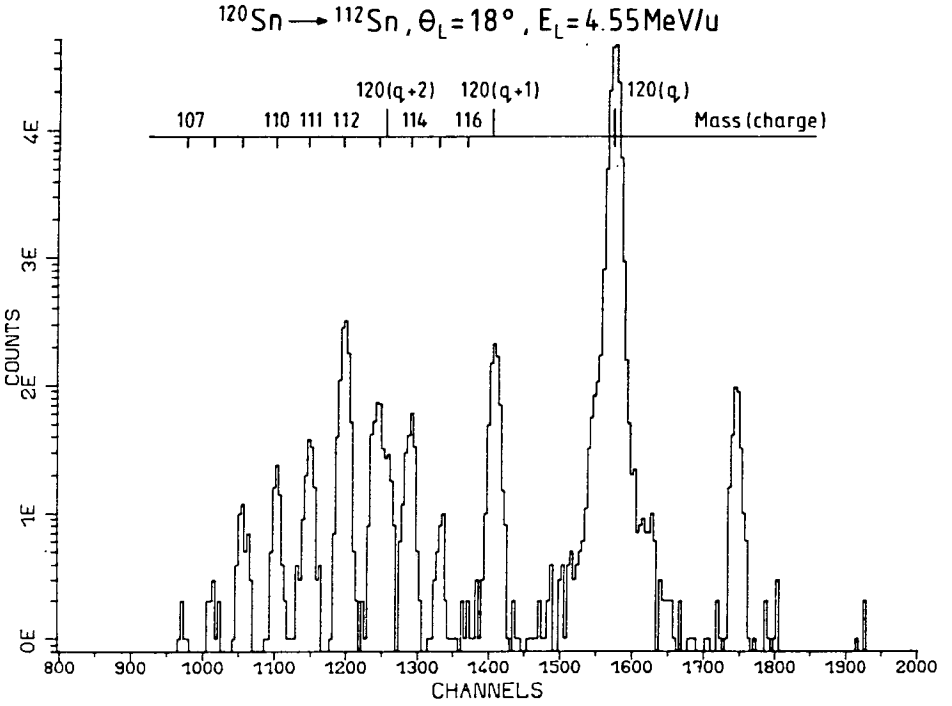

Figure 7 The mass spectrum for Sn isotopes observed in the $^{112}Sn + ^{120}Sn$ reaction at $E_{lab} = 546$ MeV and $\theta_{cm} = 144°$. A mass resolution $m/\Delta m \approx 250$ was achieved. Reproduced from Ref. 12.

tion detection of the deexcitation γ rays in coincidence with the scattered ions (32–35). Coincident detection of the scattered ions allows selection of the grazing trajectories of interest and provides the information needed to correct the observed deexcitation γ rays for the large Doppler shifts manifest in heavy-ion reactions. Arrays of Compton-suppressed Ge detectors are ideally suited for such work.

Figure 9 shows a typical γ-ray spectroscopy experimental setup for the study of nucleon-transfer between heavy nuclei. A large solid-angle array of position-sensitive parallel-plate avalanche counters is used to detect both the scattered and recoiling nuclei in kinematic coincidence, as well as in coincidence with deexcitation γ rays; thus it provides measurements of scattering angles and time-of-flight difference. The total kinetic energy loss (TKEL) or Q value and the approximate masses of both residual nuclei can be derived by assuming two-body kinematics. The angle and time resolution achieved lead to a mass resolution of $m/\Delta m \approx 10$, which is only sufficient to separate projectile-like scattered nuclei from recoiling nuclei.

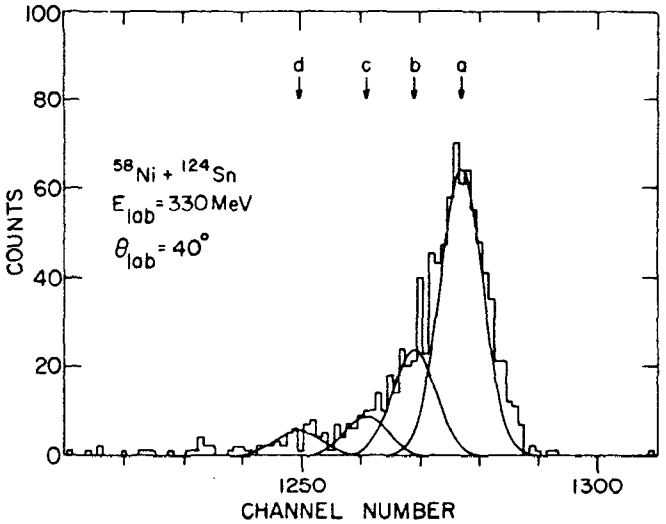

Figure 8 Magnetic rigidity spectrum for elastic and inelastic yields from $^{124}Sn + ^{58}Ni$ at $E_{lab} = 330$ MeV and for the $q = 22^+$ charge state. Indicated are positions of the elastic peak (*a*) and calculated positions for peaks at excitation energies $E^* = 1.3$, 2.6, and 4.5 MeV, denoted by *b*, *c*, and *d*, respectively. An energy resolution ~ 1.5 MeV is achieved. Reproduced from Ref. 28.

The real identification of the residual nuclei and final states is through the detection of the deexcitation γ decay with resolution of a few keV. The use of the measured Q value together with measured neutron multiplicity in these reactions is discussed below.

In principle it is possible to identify the final states and species of both residual nuclei by simultaneous observation of deexcitation γ rays from both nuclei. The Doppler correction can be made from the measured kinematics. Doppler-corrected coincident γ-ray spectra are simple and clean (Figure 10) but their statistics are inadequate for practical applications in the reactions investigated to date. This powerful technique will become viable with the increase in detection efficiency expected (two orders of magnitude) for the next generation of γ-ray detector arrays, such as the Gammasphere (36).

A deficiency of the γ-ray technique is that it selects only part of the total transfer cross section; that is, it misses the population of the ground states or states deexcited by internal conversion. This feature has been exploited to determine the ground-state cross sections from comparison of complementary studies using magnetic spectrometers (12) and γ-ray detection (13).

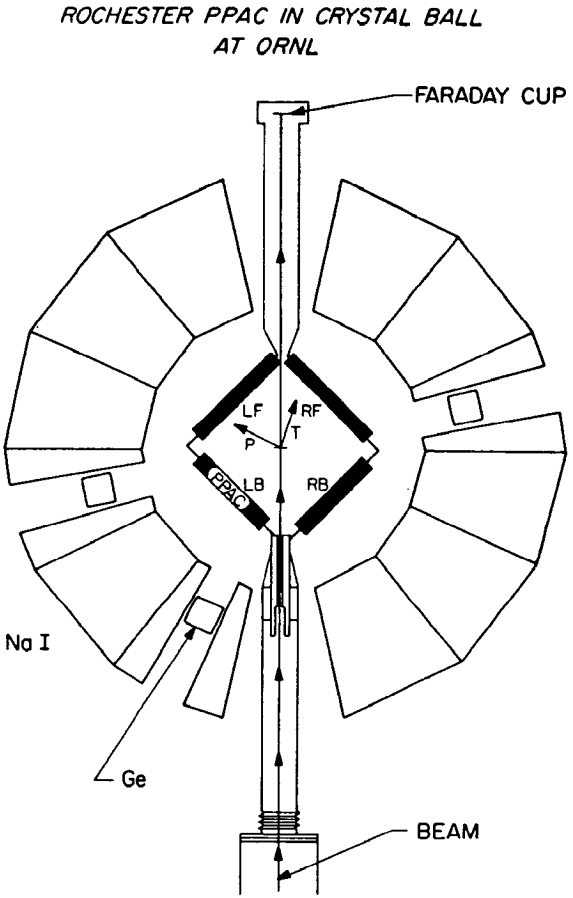

Figure 9 Cross-sectional view of an experimental setup in which an array of position-sensitive parallel-plane avalanche counters (PPAC) is enclosed by the 4π Spin Spectrometer comprising NaI and Compton-suppressed Ge elements (37). The Spin Spectrometer has an inner radius of 178 mm and a shell thickness of 178 mm.

The most important advance in the study of heavy-ion transfer with the γ-ray detection technique has been the use of multi-element 4π solid-angle γ-ray detectors. The additional information—in particular, the total energy and multiplicity of deexcitation γ-ray emission—specifies approximately the region of spin and energy of the entry states. This is essential information for many applications. Both the Oak Ridge National Laboratory Spin Spectrometer (37), which consists of 72 NaI detectors covering a 4π solid angle, and the Heidelberg Crystal Ball (33) have been exploited

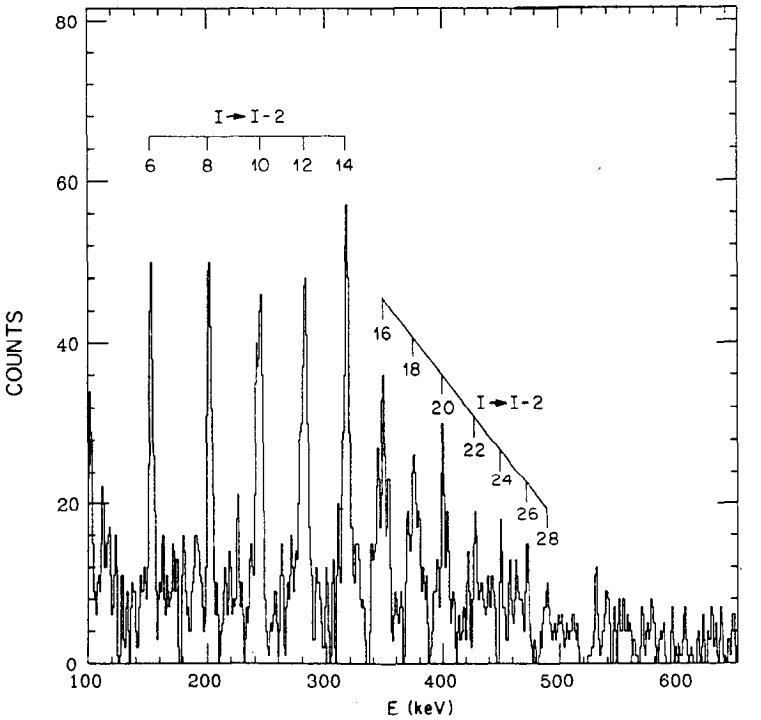

Figure 10 The two-fold γ-ray spectrum integrated over a scattering angle $45° < \theta < 75°$ for the reaction ^{235}U + 1394-MeV ^{206}Pb with sum gated on the $8^+ \rightarrow 6^+$, $10^+ \rightarrow 8^+$, and $12^+ \rightarrow 10^+$ transitions of ^{234}U (26). The integers are the initial spins of transition.

for such studies. It is typically necessary to replace some of the NaI elements by Compton-suppressed Ge detectors in order to resolve and identify the exit channels. The time and energy for each NaI element are recorded for those events satisfying a kinematic coincidence of the two scattered ions, with further requirement of at least one γ ray detected by one of the Ge detectors. The true summed γ-ray energy, E, and multiplicity, M (see Figure 11), are extracted from the measured summed energy, H, and the number of photons registered, k, by an unfolding procedure that accounts for photon scattering between NaI elements, two photons detected in a single element, gaps in the spectrometer caused by substitution of Ge detectors, etc (37).

High-resolution γ-ray spectra for the reactions ^{161,162}Dy + 637-MeV ^{116}Sn are shown in Figure 12. The characteristic discrete γ rays used to identify the inelastic and neutron transfer exit channels are marked.

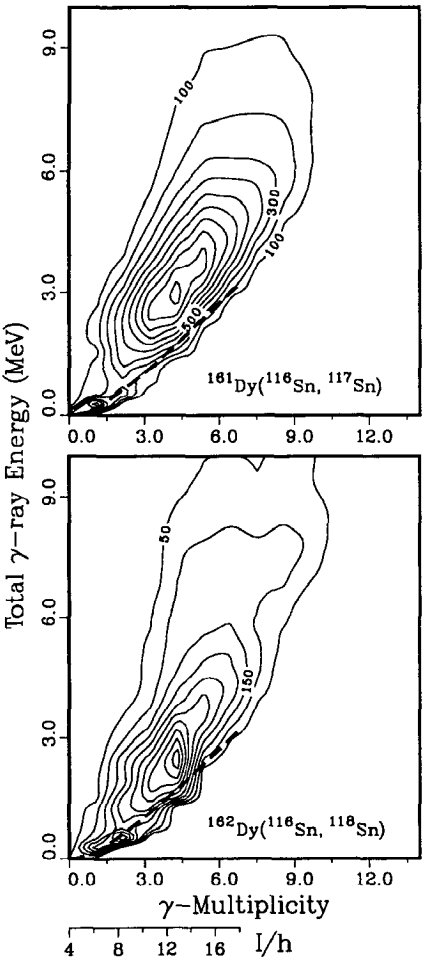

Figure 11 The unfolded total energy-multiplicity spectra from the Spin Spectrometer (37), gated around the grazing angle, for ^{160}Dy populated in one- (*top*) and two-neutron (*bottom*) pickup reactions with a Sn beam at $E_{lab} = 637$ MeV. The *dashed lines* are the approximate yrast levels of the ^{160}Dy assuming no projectile excitation. The angular momentum scale (I/h) is valid only for the Dy yrast line, with no Sn excitation.

Projections of the measured summed γ-ray energy from the Spin Spectrometer NaI elements for the quasi-elastic channels, which were selected by gating on the appropriate γ peaks in the Ge spectrum, are shown in Figure 13. The discrete structure for the low-excitation region is visible, with an energy resolution on the order of 100 keV below 2 MeV of total excitation energy.

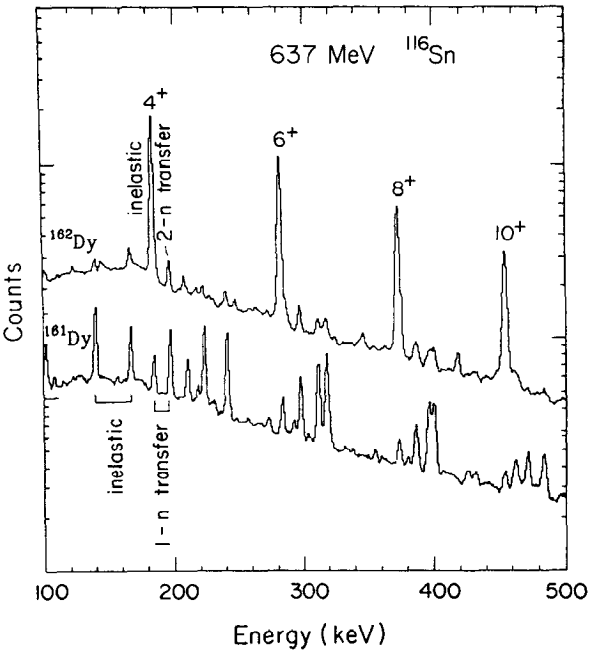

Figure 12 Ge spectra integrated over the grazing angle for the reactions ^{161,162}Dy+637-MeV Sn. The ^{162}Dy inelastic transitions and ^{160}Dy transitions from two-neutron pickup are seen in the *upper plot*. Both the ^{160}Dy (one-neutron pickup) and ^{162}Dy (one-neutron stripping) transitions, as well as the ^{161}Dy inelastic lines, are apparent in the *lower plot*.

The NaI elements of the Spin Spectrometer also provide a measure of the neutron multiplicity (K_n) because of the time-of-flight difference between the γ ray and neutron. A close correlation is observed between the deep-inelastic events, indicated by the large negative Q value from the charged-particle detectors, and neutron multiplicity $K_n > 1$. The correlation shows that this technique allows meaningful gates to be set to minimize the contamination of nucleon transfer channels by deep-inelastic and other large energy loss processes.

4. EXPERIMENTAL RESULTS

4.1 *Neutron Transfer*

4.1.1 GENERAL FEATURES FOR ONE- AND TWO-NEUTRON TRANSFER A structureless bell-shaped angular distribution for the cross section is the most distinct feature for quasi-elastic few-nucleon transfer between heavy nuclei. Figure 14 shows the cross sections in several quasi-elastic channels

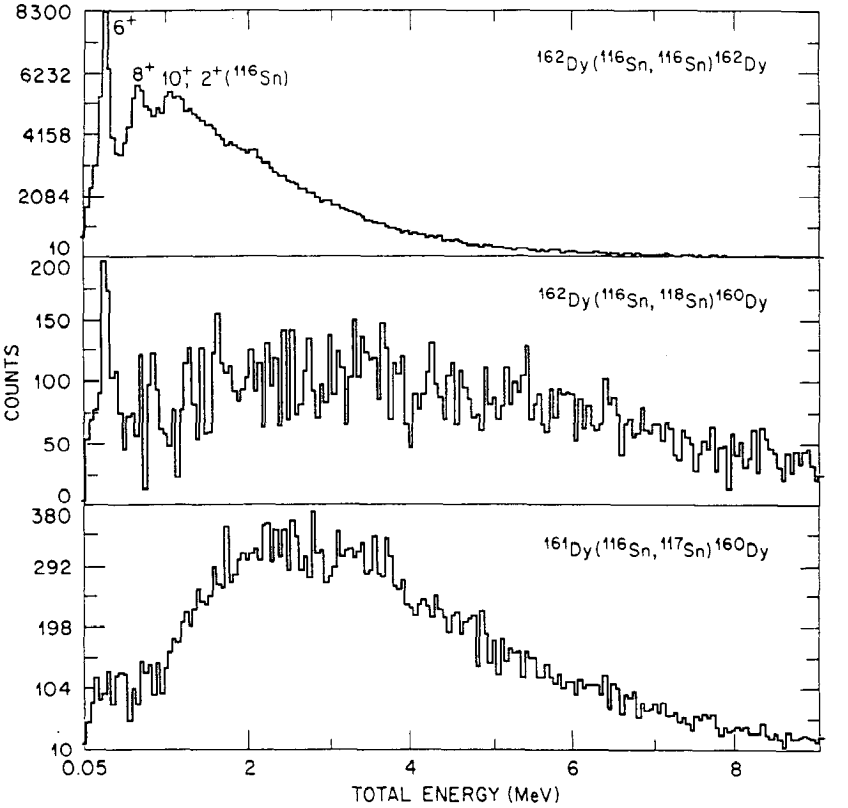

Figure 13 The total energy of NaI elements of the Spin Spectrometer (37) for the inelastic (*top*), for the one- (*bottom*), and for the two-neutron (*middle*) pickup channels for the reaction ^{161,162}Dy+637-MeV ^{116}Sn. Discrete structure in the lower end of the total energy spectrum is visible.

for the reaction ^{208}Pb+375-MeV Ni (38). The cross section for neutron transfer channels as a function of scattering angle rises rapidly because the transfer probability grows as the internucleus distance decreases with increasing scattering angle. The rapid falloff at even larger scattering angles is caused by the competition with other reaction channels that open when significant overlap occurs between the two nuclei. The peaking of the cross section around the grazing angle is a strong indication that the quasi-elastic neutron transfer is a surface process.

Other general systematics are related to the dependence of the total cross sections on the ground-state Q value, mentioned in Section 2.1.

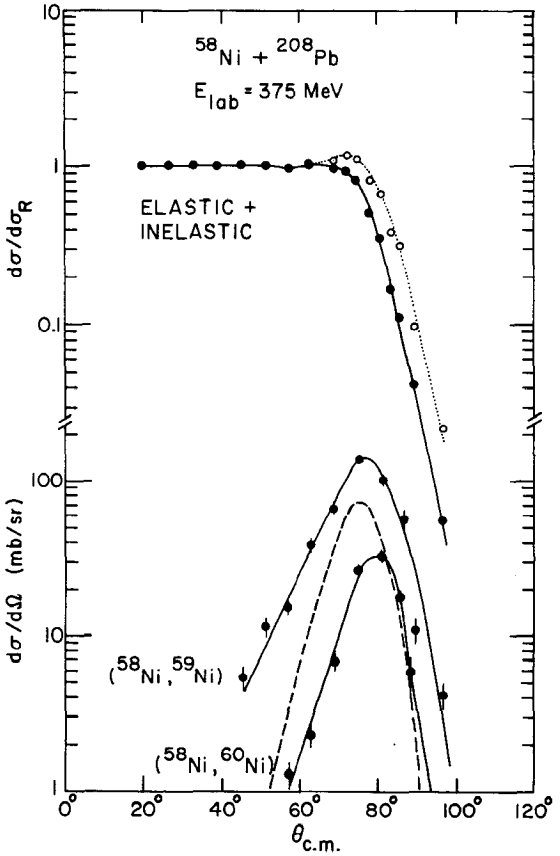

Figure 14 Angular distribution for elastic (including inelastic with excitation up to 3 MeV) (*upper*) and for one- and two-neutron pickup channels (*lower*) for the reaction ^{208}Pb+ ^{58}Ni (*filled circles*). The *solid lines* serve to guide the eye. The *dashed line* at the bottom is the result of DWBA calculation for one-neutron pickup as described in the text. The *open circles* and the *dotted line* result from adding all neutron transfer channels to the elastic and inelastic data. Reproduced from Ref. 38.

Data for one-neutron transfer over a wide range of projectile and target combinations, after correction for the binding energy of the transferred neutron in the entrance and exit channels, can be correlated well by integrating over the whole spectrum with a Gaussian Q-value "window" (see also Equation 8):

$$\sigma(Q_{gg}) = N \int_{-\infty}^{Q_{gg}} \exp[-(Q-Q_{opt})^2/2\Gamma^2]\,dQ, \qquad 18.$$

where N is a normalization constant containing all the information of the spectroscopic factors, Γ is the width of the Q window, and $Q_{opt} = 0$ for neutron transfer (19). Similar systematics are also found for the two-neutron transfer channel (39) and for systems involving deformed nuclei (13). This observation demonstrates that the total cross section for neutron transfer at energies around the Coulomb barrier is governed primarily by the Q-value matching conditions and by the number of states accessible to this reaction channel. A sum-rule limit for one- and two-particle strength appears to be of more importance rather than the details of nuclear structure for each individual state.

The importance of nuclear structure to the reaction mechanism for neutron transfer was illustrated by recent high-energy-resolution measurements, via γ-ray spectroscopy, on systems involving deformed nuclei (5, 32, 40). Figure 11 shows the unfolded total energy vs multiplicity plots, equivalent to a representation of entry states, in one- and two-neutron transfer channels for the reaction ^{161,162}Dy + 637-MeV ^{116}Sn. Two maxima are observed in Figure 11 (see also Figure 13): One, located at low energy and multiplicity and containing 10–20% of the total cross section, has a pattern similar to that of the inelastic channel and corresponds to the population of the ground-state band by removing the valence neutron or neutrons from Dy. The other one, located at higher energy-multiplicity and about 1–2 MeV about the yrast line, has a dominant share ($\sim$80–90%) of the total cross section, and is believed to be dominated by the population of two-quasi-particle bands formed by removing deeper-lying neutron or neutrons from the target nucleus. The contribution of projectile excitation blurs the distribution in energy-multiplicity. In fact, this structure is related to the Q-value matching condition, and to the nature of the surface process for transfer reactions. As the nuclei rotate faster, the rotation alignment produced by the Coriolis force causes deeper-lying high-j single-particle orbits to "surface" close to the yrast sequence, where they are within reach of the allowed Q window for neutron transfer (32).

Populating high-spin states is another important feature of neutron transfer reactions with deformed nuclei. For example, discrete transitions with spin up to 18^+ for the rare earth region (32) and 26^+ for the actinide region (41) have been observed in one-neutron transfer by using a Ni beam near the barrier. A "cold" reaction mechanism for neutron transfer involving actinides, similar to that found for rare earths, has been confirmed by measuring the total energy and multiplicity in the well-matched Ni-induced reactions (41). This feature, plus the "cleanliness" of the resulting γ-ray spectrum, which has little contamination from competing reaction channels (see Figure 10), makes such reactions an attractive alternative for populating high-spin states in actinide nuclei inaccessible by other

means. A recent study of ^{234}Th, excited via the two-neutron stripping reaction, is another example (42).

4.1.2 QUANTITATIVE COMPARISONS FOR ONE-NEUTRON TRANSFER Prior to a discussion of multinucleon transfer in heavy-ion reactions, it is necessary to examine the extent to which the conceptually simpler process of one-nucleon transfer is understood. A quantitative understanding of few-nucleon transfer between heavy nuclei turns out to be difficult because of (*a*) the lack of sufficient energy resolution to separate the individual states experimentally, and (*b*) the lack of theoretical models other than the distorted-wave Born approximation for interpreting the data. Even the DWBA is of limited use because it is based on perturbation theory. Nevertheless, several authors have compared experimental data with DWBA calculations for one-neutron transfer between heavy nuclei, where most of the spectroscopic factors needed for the calculations are available experimentally (12, 13, 38).

Figure 15 shows the measured Q-value spectrum for one-neutron transfer in the reaction ^{208}Pb+375-MeV ^{58}Ni (38). The shaded area is the smoothed energy spectrum, summing over 24 transitions, calculated using the DWBA including the states where most of the spectroscopic factor strength lies: the $3/2^-$ (ground state), $5/2^-$, $1/2^-$, $9/2^+$ states in ^{59}Ni and the $1/2^-$ (ground state), $5/2^-$, $3/2^-$, $13/2^+$, $7/2^-$, $9/2^-$ states in ^{207}Pb. The

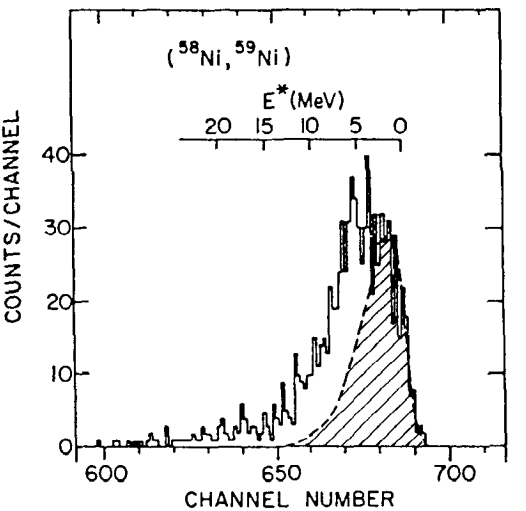

Figure 15 Energy spectrum for one-neutron pickup in the reaction ^{208}Pb+58Ni at E_{lab} = 375 MeV and θ_{lab} = 65°. The *shaded area* represents the smoothed energy spectrum for a total of 24 transitions calculated using DWBA as described in the text. From Ref. 38.

lower end of the excitation energy spectrum is well reproduced. The excess experimental strength for the higher excitation energy may be a consequence partially of ignoring inelastic excitation and partially of the truncated space used in the calculation. This example illustrates the difficulty inherent to the study of nucleon transfer reactions between heavy nuclei, which become less "transparent" compared with similar reactions using light ions as probes.

The next example shows results for a one-neutron transfer reaction between ^{117}Sn and ^{112}Sn at a bombarding energy of 570 MeV, from a measurement using the γ-ray technique (13). Figure 16 shows the population of the $5/2^+$ state in ^{113}Sn, which is deduced from the γ-ray yield of the transition $5/2^+ \rightarrow 7/2^+$ at 332 keV. There is little evidence of appreciable feeding to this state from states in the known level scheme. Since the measurement is "inclusive" in nature, the transfer strengths to various states of the other partner, namely ^{116}Sn, have to be summed for the comparison. The contributions from the ground state (0^+) and excited 0^+, three 2^+, two 4^+, 5^-, 6 states of ^{116}Sn, calculated by DWBA with the measured spectroscopic factors, are shown by various lines in Figure 16. The sum of all these transitions is shown by the dashed line. The angular

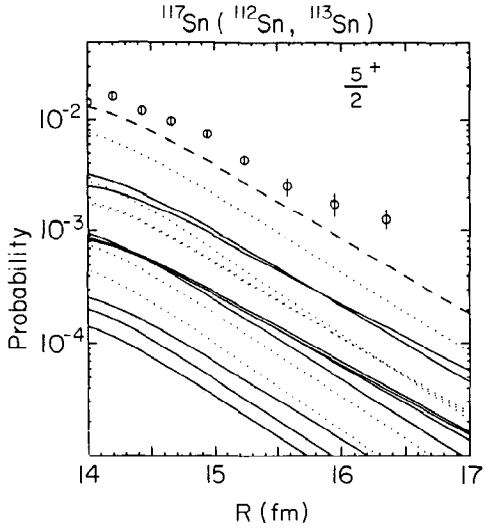

Figure 16 Constituents of a DWBA calculation of probability vs the distance of closest approach for the $5/2^+$ state in ^{113}Sn populated by the ^{117}Sn(^{112}Sn, ^{113}Sn) reaction at $E_{lab} = 570$ MeV. Constituents contributed by the component $J = l - \frac{1}{2}$, the total angular momentum carried by the transferred neutron, are shown as *dotted lines*; those contributed by the component $J = l + \frac{1}{2}$ are shown as *solid lines*. The *dashed line* is the sum of nine transitions, as described in the text.

distribution is well reproduced, while the predicted absolute magnitude is about a factor of two too low. Similar agreement is also reached for both the $3/2^+$ state in ^{113}Sn, identified by the transition $3/2^+ \rightarrow 1/2^+$ at 498 keV. For the first 2^+ state in ^{116}Sn, identified by the transition $2^+ \rightarrow 0^+$ at 1294 keV, the summed transfer strengths contributed from the $1/2^+$ (ground state), $3/2^+$, $5/2^+$, $7/2^+$, $11/2^+$, $7/2^-$ states in ^{113}Sn plus its own feeding, a total of 48 transitions, are in reasonable agreement with the data. The total cross section for one-neutron transfer between ^{112}Sn and ^{120}Sn is overestimated by only 50% relative to the experimental value in a DWBA calculation that uses known spectroscopic information (12). Note that the binding energy of a neutron in nuclei alone can account for the observed slope of the transfer function at large separation distances under the semiclassical decription. Thus, the DWBA seems to give a correct overall qualitative description of the reaction mechanism for one-nucleon transfer between spherical heavy nuclei, and it reproduces the total cross section to within a factor of two.

The existence of strong inelastic excitation for heavy-ion collisions with deformed nuclei invalidates the DWBA approach for the calculation of nucleon transfer reactions, and thus the coupled-channel Born approximation or coupled reaction channels method is probably necessary (18). Little work has been done on this kind of calculation for very heavy-ion transfer reactions but is desperately needed to interpret the experiments discussed in this review.

4.1.3 QUEST FOR ENHANCEMENT IN TWO-NEUTRON TRANSFER One of the most significant aspects of two-nucleon transfer reactions between heavy nuclei is the study of "superfluidity" of nuclei. The study of pairing enhancement reveals the dynamical aspects of pairing correlations in nuclei. The study of multiple-pair nucleon transfer between two heavy nuclei at an energy below the Coulomb barrier may be similar to that of a supercurrent between two superconductors separated by an insulator.

The spherical, proton-closed, Sn nuclei are ideal candidates for the study of neutron superconductivity in nuclei. Neutron transfer reactions between ^{112}Sn and ^{120}Sn have been studied with the magnetic spectrometer (12) in an "inverse" kinematic arrangement. The transfer probabilities for one and up to four neutrons at bombarding energies of 510, 546, and 576 MeV were measured and are shown in Figure 17. A parallel shift of the P_{2n} curve relative to the prediction P_{1n}^2 by a factor of about 3 is observed. Finite energy resolution prohibits the isolation of the ground-state to ground-state ($0^+ \rightarrow 0^+$) transfer component in the two-neutron transfer channel. The enhancement must be defined relative to some "single-particle unit," which is obtained from the analysis as a typical one-neutron transition between well-defined states. An enhancement of about 300 is

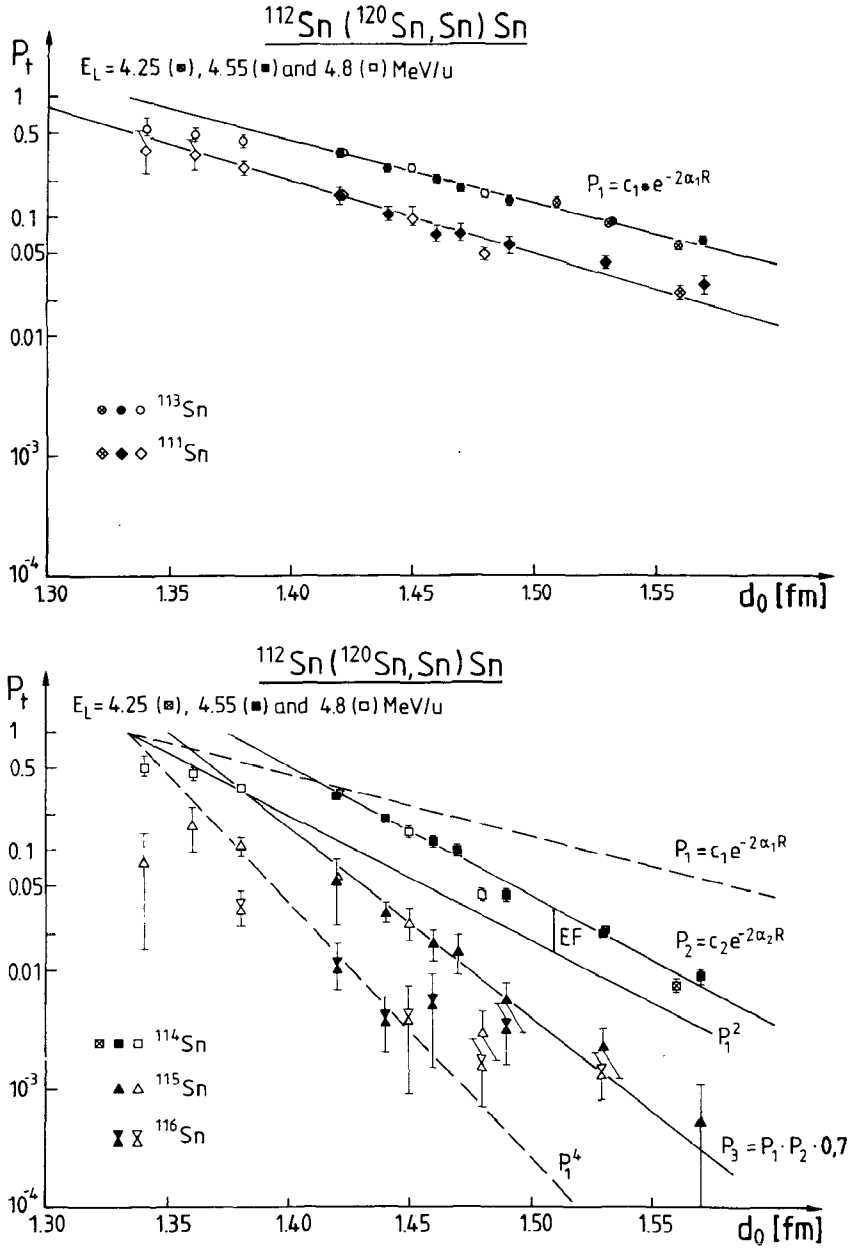

Figure 17 Measured transfer probabilities (transfer function) for one- (*top*) up to four-neutron (*bottom*) transfer in the system $^{112}Sn + ^{120}Sn$, as a function of the overlap parameter d_o. Data at three energies (4.25, 4.55, and 4.8 MeV/nucleon) are shown. Reproduced from Ref. 12.

obtained indirectly by considering the phase space in one- and two-neutron transfer reactions (12). Recent measurements on neutron transfer between ^{118}Sn and ^{112}Sn, made with the γ-ray technique (13), complement the spectrometer result by measuring the cross section of transfer to the excited states and ignoring the transfer between the ground states. Figure 18 shows the total probability for two-neutron transfer, as a function of the overlap parameter d_o, for the system ^{112}Sn + ^{120}Sn, plus the probabilities for the $2^+ \rightarrow 0^+$ transition for both projectile, P_t^{pro}, and target, P_t^{tar}, nuclei in the system ^{118}Sn + ^{112}Sn. The probability for the transfer between the ground states of Sn nuclei thus can be deduced from the above information.

The data shown in Figure 18 for $P_t(0^+ \rightarrow 0^+)$ are derived from the measured P_t(tot) after correcting for the slightly different Q_{gg} in the two systems. An enhancement of about 760 is obtained from this extracted probability for the $0^+ \rightarrow 0^+$ transfer and from the ground-to-ground one-neutron transfer strength (see Figure 16) estimated by a DWBA calcu-

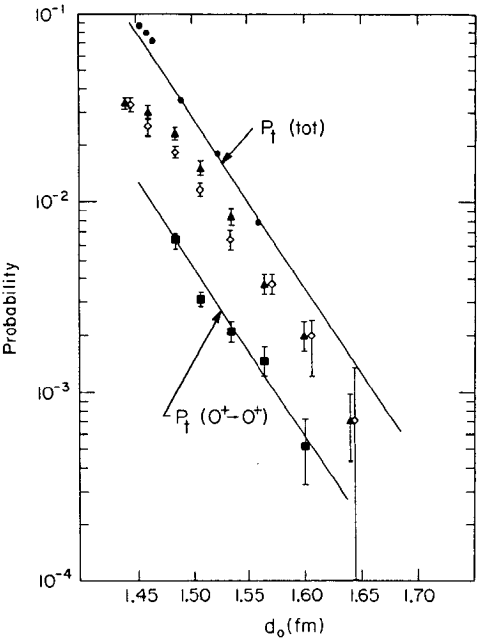

Figure 18 The total probability for the reaction ^{112}Sn(^{120}Sn,^{118}Sn) at $E_{lab} = 546$ MeV, measured with the magnetic spectrometer (*filled circles*) (12). Also shown are the probabilities for the $2^+ \rightarrow 0^+$ transition for both ^{114}Sn (*triangles*) and ^{116}Sn (*diamonds*) from the reaction ^{118}Sn(^{112}Sn,^{114}Sn) at $E_{lab} = 570$ MeV (13). The extracted ground-state to ground-state transfer probability is shown with *squares*. The *solid lines* are the best fits to the experimental data.

lation. A correction factor of 3 has been included to account for the inelastic excitation. This extracted enhancement is comparable with that mentioned earlier; it is believed to be accurate to within a factor of 2, since a 30% change in $P_t^{pro(tar)}$, which is roughly the uncertainty of the measurement, alters the enhancement by about 40%. This value is also consistent with the enhancement 100–1000 predicted for the $0^+ \rightarrow 0^+$ two-neutron transfer between Sn nuclei (10, 11).

The observed slope of the transfer function for the Sn+Sn system in the subbarrier region is close to twice that for one-neutron transfer; it can be reproduced by DWBA calculations, and by a semiclassical description, assuming ground-state binding energies for the transferred neutrons. This indicates a cold pair transfer. For two-neutron transfer reactions with deformed nuclei, the situation is different: the slope of the transfer function in the subbarrier region is close to that for one-neutron transfer, but simple energy arguments predict that it should be twice as large (33–35, 40, 43). This "slope anomaly" in deformed nuclei must be addressed before we can discuss enhancement in these systems.

Isolation of the states with different intrinsic structure turns out to be the key to understand the slope anomaly (5). As seen in Figures 11 and 13, the members of the ground-state band are partially separated from states with excited two-quasi-particle configurations in the two-neutron transfer channel for the system ^{162}Dy + ^{116}Sn. Figure 19 shows the transfer functions for the population with excitation energy less than 1.2 MeV, that for the population with excitation energy greater than 1.2 MeV, and the total. In contrast to the population of higher excitation energy, where the transfer function follows an exponential decay with a slope ($\alpha \approx 1.0$) approaching the expected value (~ 1.2), the transfer function for the population of the low-lying states exhibits an oscillating structure. This oscillating structure is well reproduced by a recent calculation (4) in which the transfer of a neutron-pair with relative angular momentum 0, 2, and 4 is included in the calculation (see Section 2.5). In the semiclassical picture, this is related to the interference between scattering amplitudes from two different orientations of deformed nuclei that lead to the same final spin, which was predicted earlier by Guidry et al (44). The observation of this interference phenomenon may indicate that the particle-particle correlations are such that the transfer of two particles to the ground band does not destroy the phase information carried by the deformed rotor. The ^{208}Pb(^{64}Ni,^{62}Ni)^{210}Pb two-neutron transfer reaction (45), which has a highly negative Q_{gg} leading to population of only low-lying states, also exhibits a slope anomaly.

The strong coupling between the members of the ground-state band in the inelastic excitation for heavy-ion collisions involving deformed nuclei

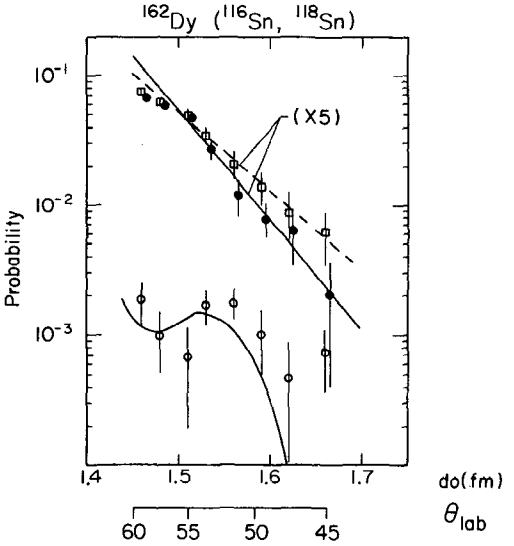

Figure 19 The probability for two-neutron transfer to states with an excitation energy below 1.2 MeV (see Figure 13) (*open circles*), above 1.2 MeV (*filled circles*), and the sum of these two (*squares*) for the reaction $^{162}Dy + ^{116}Sn$ at $E_{lab} = 637$ MeV. The *dashed* and *solid lines* are the best fits to the data respectively for the total and for the states with higher excitation energy (> 1.2 MeV). The undulating *solid curve* is the summed probability of 4^+, 6^+, and 8^+ states from the calculation of Ref. 4.

imposes great difficulty in defining a simple enhancement factor for pair transfer. Indeed, the idea of a simple average enhancement factor is probably a qualitative concept, at best, for such systems. The quantitative information about correlations in these cases must be extracted from a comparison of data with sophisticated calculations. It can be argued that the transfer strength to the ground-state band in deformed nuclei is representative of that to the ground state in spherical nuclei, i.e. a group of states are involved in determining the enhancement. The enhancement factor cannot yet be quantitatively estimated because of the difficulty of determining P_{1n} either experimentally or theoretically for deformed nuclei. However, there is an interesting feature of the data shown in Figure 19: whereas the ground-state band population is only 10% of that for populating two-quasi-particle states for $d_o < 1.5$ fm, the ground band and two-quasi-particle bands are populated roughly equally at $d_o \approx 1.6$ fm. That is, the relative importance of the ground-state band population increases markedly at large separation distance. Furthermore, at $d_o \approx 1.6$ fm the ground-band population is comparable to that for the $P_t(0^+ \rightarrow 0^+)$ in Sn+Sn shown in Figure 18. These data suggest that the two-neutron

transfer to the ground band is appreciably enhanced at large separation in these collisions.

4.2 *Proton Transfer*

Before discussing the results for proton transfer, some general remarks are necessary to emphasize the similarities and differences between neutron and proton transfer.

The proton bound states in the asymptotic region (outside of the nucleus) have for the same binding energy a steeper decay of the wave function because of the presence of the Coulomb interaction. Thus for the same internuclear distance (overlap of densities) the probability of transferring a proton is typically a factor 3–5 smaller. The same conclusion is drawn from the inspection of the two-center potentials shown in Figure 20 and discussed below. However, the transfer probabilities for neutrons and protons reach equal magnitudes for overlap configurations that show the same geometry of the interior barrier. It was found that $P_t(1p) \approx P_t(1n) \approx 0.1$ for overlap parameter $d_o(1p) \approx 1.4$ fm and $d_o(1n) \approx 1.55$ fm (47).

Studies of multiproton transfer are only possible if the Q values are matched so as to obtain sizable cross sections for one- and two-pair transfer. Such studies have been done for spherical nuclei having closed neutron shells (47, 48) and open proton shells, where enhancements for transitions between pairing rotational bands of protons can be expected. One example is discussed here.

In the system $^{144}Sm + ^{88}Sr$ at energies below the Coulomb barrier [$E = 4.70$ MeV/nucleon, with smallest d_o at $d_o(180°) = 1.39$ fm], the transfer of up to four protons has been observed (14, 47). The measurement was performed with the magnetic spectrometer at the UNILAC of GSI by detecting recoil events of target-like products at small angles. Complete particle identification was achieved. Almost the same energy width is observed for one- and two-proton transfer, whereas an increasing overall energy loss up to about 20 MeV is observed for further transfer steps (14). This energy loss is most likely associated with the excitation of neutron configurations, because neutron exchange can occur unhindered as a result of the low interior barrier. In Figure 21 we show the experimental transfer functions for one- up to four-proton transfer. An increasing slope of the functions is observed, as predicted for cold multinucleon transfer. In the present case, however, the individual one-proton transfer steps are not equal because of the changing Coulomb interaction and Q value for each transfer step.

Inspecting Figure 21, we find that the pair transfer is enhanced by a factor of 9 compared with the square of the one-proton transfer, and the enhancement is kept in the second pair (four-proton transfer); the latter is

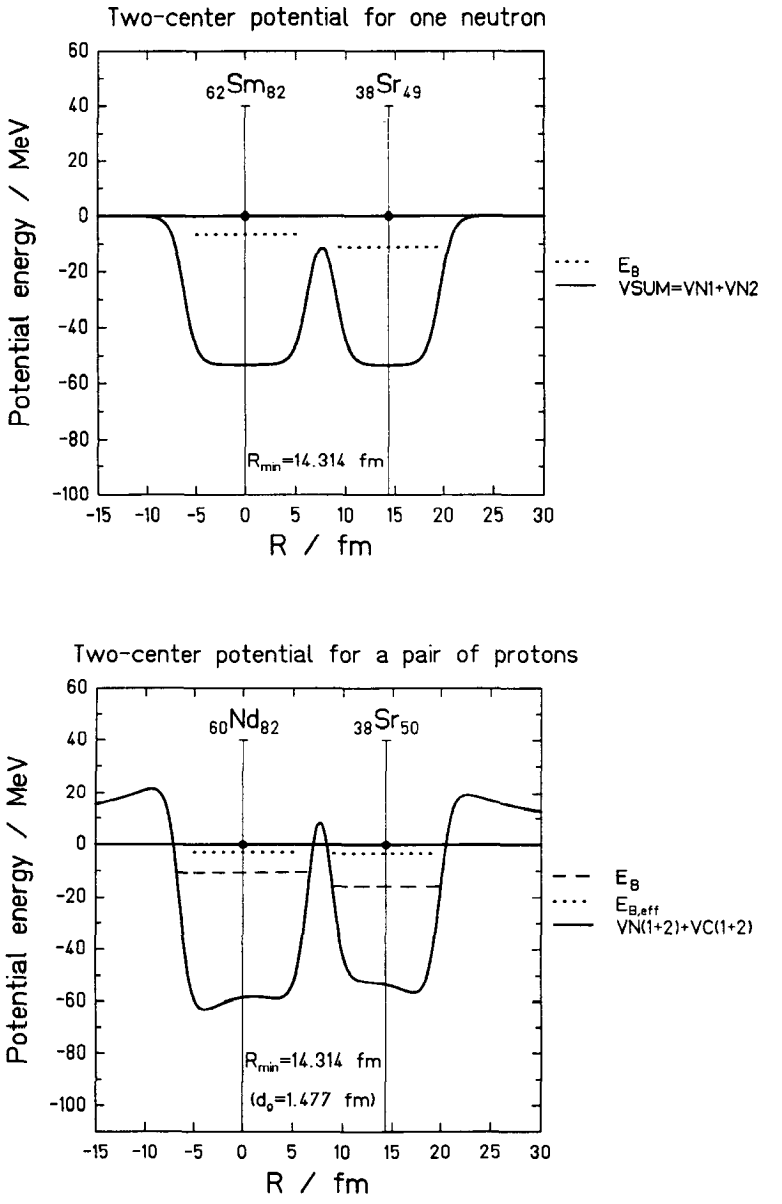

Figure 20 Two-center potentials for neutrons (one neutron) and protons (a proton pair) for the system $^{144}Sm + ^{88}Sr$ at the same internuclear distance. The level of the least bound nucleon (or nucleon pair) is indicated by *dotted lines*.

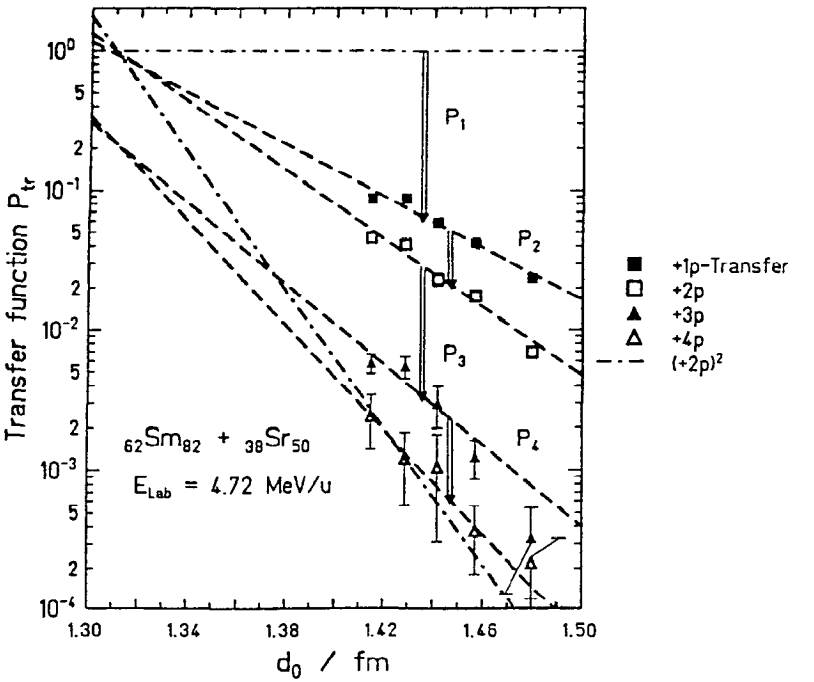

Figure 21 Measured transfer probabilities for one up to four protons in the system $^{144}Sm + ^{88}Sr$, as a function of the overlap parameter d_o. Note the strong odd-even staggering indicated by the *open arrows*. The *dashed curves* are fitted exponentials showing the increasing slopes. From Ref. 14.

rather well reproduced in magnitude and slope by the square of the two-proton transfer function. Reducing the measured cross sections to the equivalent of a single transition by estimating the phase space for one- and two-proton transfers gives a final enhancement of about 500, as in the case of Sn isotopes. We therefore can call this transfer of multiple pairs a supercurrent between the two superfluid configurations in ^{88}Sr and ^{144}Sm. Cold multiple proton pair transfer has also been observed in even heavier systems such as $^{144}Sm + ^{208}Pb$ (48).

An important aspect already discussed in the context of pair transfer is the two-center potential configuration for the bound nucleons and Cooper pairs. For the protons the Coulomb interaction creates an interior barrier, which persists to smaller overlap distances than for neutrons. Figure 20 shows the situation for proton pairs as well as for neutrons in the $^{88}Sr + ^{144}Sm$ system, for a distance corresponding to a d_o value of 1.47 fm. The interior barrier is still higher than the level of the macroscopic proton pair states, and cold transfer requires tunneling between the two potential

wells. In contrast, the interior barrier has vanished for neutrons. This point is further discussed in the next section.

4.3 *Multiple-Pair Transfer and Aspects of the Nuclear Josephson Effect*

The possibility of bringing the superfluid nuclei into contact and observing phenomena related to the Josephson effect has stirred the imagination of many authors (8–11). Two aspects of such contact between two superfluid nuclei are discussed here. The first is the case of strong coupling where multiple exchange of pairs can be anticipated with sizable probability. This situation has been explicitly discussed by Hara (49) and Dietrich (50).

The predictions in this work have been tested for neutron transfer in ^{112}Sn+^{120}Sn (12). The main limitations for realistic systems come from the absorption into deeply inelastic collisions, once the interior barrier for neutrons and neutron pairs has vanished. In the present case, a probability of 0.5 for pair transfer is reached at a distance corresponding to $d_o = 1.40$ fm. At this distance the absorption probability is 90%; a flux oscillation is thus difficult to observe. In a coupled-channel calculation using the experimentally observed pair transfer strength to represent one transition, a flux oscillation of 30–50% because of multiple (two) pair transfer back to the elastic channel can be predicted for ^{112}Sn+^{120}Sn at a higher energy than that of the case presented, $E_L = 590$ MeV. This is illustrated in Figure 22, where coupled-channel calculations for two channels (the elastic and the two-neutron transfer) are shown for various energies.

This effect could be increased and observed at lower energy if the binding energy of the neutron pairs was decreased to 10 MeV. Such possibilities could be created using the most neutron-rich isotope (^{124}Sn) as the target and a possible radioactive beam of ^{130}Sn, for which an overall increase of the pair transfer probability by a factor of 3–5 relative to the ^{112}Sn+^{120}Sn case can be expected.

Multiple-neutron pair transfer has also been discussed in the weak coupling limit $P_t(1 \text{ pair}) \approx 0.1$ using the macroscopic form factor approach (51). In this approach the simultaneous transfer of two pairs is a feature whose amplitude depends on the gauge phase. More conspicuous may be the influence of the Coulomb potential on the gauge phase, which can occur for proton pair transfer.

This second aspect of the nuclear Josephson effect connected to the gauge phase coupling occurs if two superconductors are brought into contact with a definite potential difference. This can be illustrated best in the context of proton pair transfer. We already discussed the matching condition for scattering orbits for the Q value. Each bound state is influenced by the Coulomb interaction, with the other center giving rise to an

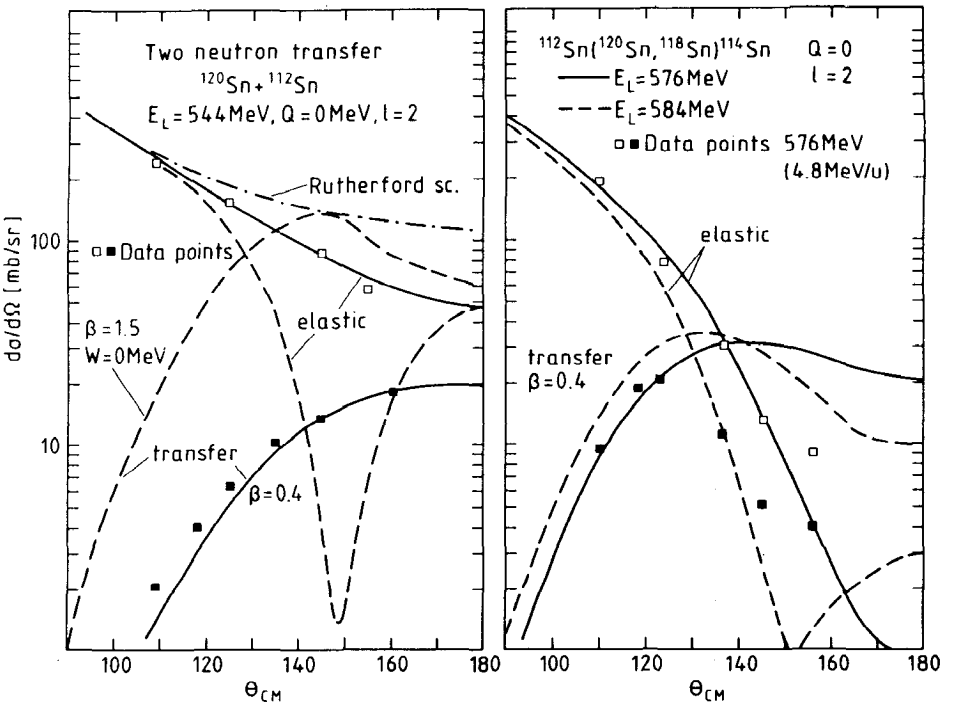

Figure 22 Data and coupled-channel calculations for the elastic and two-neutron transfer channel in the system $^{112}Sn + ^{120}Sn$. Curves for the transfer coupling $\beta = 0.4$ are shown in both panels; on the *left* (lower energy) are also shown *dashed curves* for $\beta = 1.5$. The latter exhibit a classical flux oscillation.

effective binding energy $E_i^{eff} = E_i + Z_c Z_b / R$. An effective Q value is thus obtained, $Q_{eff}(R) = (E_i + Z_c Z_b / R) - (E_f + Z_c Z_A / R) = Q + \Delta E_c$, for the process $a + A \rightarrow b + B$, with $a = b + c$, where c refers to the transferred particle. This Q value depends on the internuclear distance R, and the matching condition is simply $Q_{eff} = 0$. The situation is illustrated for $^{88}Sr + ^{144}Sm$ in Figures 20 and 23, where the shifted and unshifted position of the bound levels are indicated and the final value of Q_{eff} is shown.

For $Q_{eff} = 0$ (the matching condition also for the scattering states) we have a situation corresponding to a direct-current Josephson junction, where the potential difference ΔV across the barrier is represented by $\Delta V = Q_{eff} = 0$. For a finite Q_{eff} a situation corresponding to an alternating-current Josephson junction is obtained. Neither situation is stationary because the chemical potential will change as a function of pair number. Thus a coupled equation is obtained, which has been discussed for nuclear

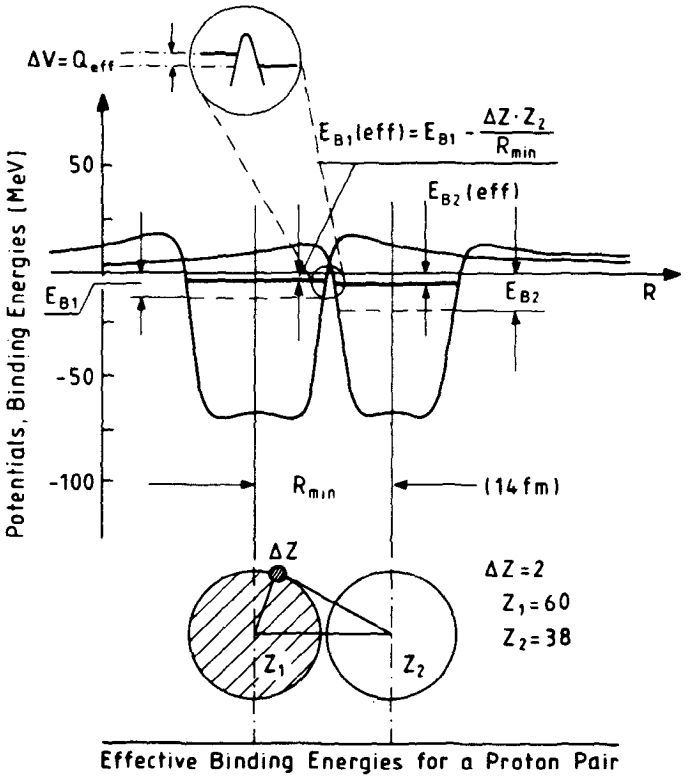

Figure 23 Illustration of the geometry of a nuclear Josephson junction (see also Figure 20). The difference in effective binding energies of the two macroscopic pairing states, each bound in its potential, represents the potential difference $\Delta V = Q_{\text{eff}}$ across the interior barrier. The height of the latter depends on the internuclear distance.

collisions by Kleber & Schmidt (52) and for cold fission by Gaudin (53). Observing various effects in this weak coupling limit may be difficult because of the short time interval in which the nuclei interact. The main features of the nuclear Josephson junction that will be observable (or have been observed) are the supercurrent of pairs in one direction or the multiple exchange of pairs in the strong coupling limit.

5. FUTURE DEVELOPMENTS

The unique features of heavy-ion-induced transfer reactions have the potential to add a new dimension to the study of nuclear structure. Unfor-

tunately, the considerable experimental and theoretical difficulties associated with such studies have delayed exploiting this technique. Recent results described in this paper point the way to exciting research opportunities in this field.

Two promising and complementary experimental techniques are being developed. The first is a particle spectroscopy method, which involves detecting both exit particles, in kinematic coincidence, with high energy and mass resolution using a magnetic spectrometer. This method has the potential of attaining an energy resolution below 1 MeV for heavy ions and, by identifying both products, will allow the measurements to be extended much further into the sub-Coulomb region without significant difficulty from target and beam contaminants. The second experimental technique exploits the Gammasphere 4π array (36), consisting of 110 high-efficiency Compton-suppressed Ge detectors, which will give more than an order-of-magnitude increase in particle-γ coincidence rate compared with the present generation of experiments, plus total energy and γ-multiplicity information. However, it is the increase (two orders of magnitude) in particle-γ-γ triple coincidence rate and the ability to perform even higher-fold coincidence experiments that will open new frontiers. These advances will allow simultaneous identification of both reaction products, or at least greatly improve the sensitivity for studying γ-ray spectroscopy in one of the product nuclei. The important discoveries in traditional high-spin γ-ray spectroscopy are a direct consequence of the improved sensitivity provided by observation of γ-ray coincidences, and similar advances can be anticipated when applied to transfer reactions.

The theoretical calculation of heavy-ion transfer reactions is a formidable task because of the many strongly coupled channels involved. Advances in computers already make it feasible to perform simplified calculations using either coupled-channel calculations or the elegant and economical semiclassical approaches. The accelerating pace of computer developments may lead in the near future to more realistic and complete reaction calculations, as well as to model calculations of spectroscopic amplitudes, etc. Such calculations are sorely needed to interpret experimental data presently available; they will be indispensable for interpreting data from the next generation of experiments.

There are many applications of heavy-ion transfer reactions to nuclear spectroscopy. One obvious possibility is to exploit the features of these reactions selectively to populate states with spin greater than 30 that are not readily populated by other reactions. This will allow γ-ray spectroscopy studies with high-efficiency detector arrays like Gammasphere. Heavy-ion transfer reactions permit the study of more neutron-rich nuclei than do fusion evaporation reactions, and the γ-ray spectra are less complicated

because of the final-state selectivity. In contrast to fusion evaporation reactions, well-matched heavy-ion transfer selectively populates states in the yrast domain and thereby suppresses the fission decay channel. This opens the opportunity of studying the spectroscopy of actinide as well as rare earth nuclei. Selective population of maximally aligned two-quasi-particle configurations by transfer reactions also has interesting spectroscopic applications. These reactions have the potential to probe, in a controlled way, nuclear structure and the damping of rotational motion (54) at nearly zero temperature through study of the quasi-continuum γ rays.

Heavy-ion transfer reactions will be exploited to probe, in a direct and sensitive way, single-particle structure and its interplay with collective degrees of freedom. It should be possible to study the localization of the spatial distribution of Nilsson orbits (44), as well as the importance of Coriolis effects on these orbits. Another potential application is to the identification of high-j orbits in actinide nuclei (55), which are of considerable interest in the predicted stability of superheavy nuclei. Finally, we note that the possibility of using highly neutron-rich nuclei from a radioactive beam facility could greatly expand the scope of the experiments discussed here, and would provide opportunities to study the spectroscopy of neutron-rich nuclei as well as the transfer reactions.

The importance of pair and multinucleon transfer reactions for studying correlations in nuclei has been emphasized in this paper. Studies to date are only a prelude to the exciting physics that should be accessible to the next generation of detectors. Studies of analogs of solid-state pairing phenomena in such reactions could provide a substantial advance in the understanding of pairing phenomena in the many-body quantal systems of interest in both nuclear and condensed-matter physics.

ACKNOWLEDGMENT

The work at the University of Rochester is supported by the US National Science Foundation. The work at the University of Tennessee and the Oak Ridge National Laboratory is supported by the US Department of Energy.

Literature Cited

1. Satchler, G. R., *Direct Nuclear Reactions*. New York: Oxford (1983)
2. Broglia, R. A., Hansen, O., Riedel, C., *Adv. Nucl. Phys.* 6: 287 (1973)
3. Panert, W., Ring, P., Gambhir, Y. K., *Nucl. Phys.* A443: 189 (1985)
4. Landowne, S., Price, C., Esbensen, H., *Nucl. Phys.* A484: 98 (1988)
5. Wu, C. Y., et al., *Phys. Rev.* C39: 298 (1989)
6. Nikam, R. S., Ring, P., *Phys. Rev. Lett.* 58: 980 (1987)
7. Berry, M. V., *Proc. R. Soc. London Ser. A* 392: 45 (1984)
8. Goldanski, V. I., Larkin, A. I., *Sov. Phys. JETP* 26: 617 (1968)

9. Dietrich, K., *Ann. Phys.* 66: 480 (1971)
10. Broglia, R. A., et al., *Phys. Lett.* 73B: 401 (1978); Broglia, R. A., Liotta, R., Nilsson, B. S., Winther, A., *Phys. Rep.* 29C: 291 (1977)
11. Weiss, H., *Phys. Rev.* C19: 834 (1979)
12. von Oertzen, W., et al., *Z. Phys.* A326: 463 (1987)
13. Kernan, W. J., et al., *Nucl. Phys.* Submitted (1990)
14. Künkel, R., et al., *Phys. Lett.* 208B: 355 (1988)
15. Alder, K., Winther, A., *Electromagnetic Excitation*. Amsterdam: North Holland (1975)
16. Bass, R., *Nuclear Reaction with Heavy Ions*. Berlin, Heidelberg: Springer-Verlag (1980)
17. Broglia, R. A., Pollarolo, G., Winther, A., *Nucl. Phys.* A361: 307 (1981)
18. Macfarlane, M. H., Pieper, S. C., *Ptolemy: A Program for Heavy-Ion Direct-Reaction Calculations*, Tech. Rep. ANL-76-11 Rev. 1, Argonne Natl. Lab., Ill. (1978)
19. van der Berg, A. M., et al., *Phys. Lett.* 194B: 334 (1987)
20. Götz, U., et al., *Phys. Rep.* 16C: 115 (1975)
21. Bayman, B. F., Chen, J., *Phys. Rev.* C26: 1509 (1982)
22. Price, C., Esbensen, H., Landowne, S., *Phys. Lett.* 197B: 15 (1987)
23. Canto, L. F., et al., *Phys. Lett.* 192B: 4 (1987)
24. Canto, L. F., et al., *Phys. Lett.* 241B: 295 (1990)
25. de Boer, J., Dasso, C. H., Pollarolo, G., *Z. Phys.* A335: 199 (1990)
26. Helmer, K. G., et al., *Annu. Rep.*, Univ. Rochester, pp. 55, 57 (1988)
27. Rehm, K. E., Wolfs, F. L. H., *Nucl. Instrum. Methods* A273: 262 (1988)
28. van den Berg, A. M., et al., *Phys. Rev.* C37: 178 (1988)
29. Cormier, T. M., *Annu. Rev. Nucl. Part. Sci.* 37: 537 (1987)
30. Betts, R. R., In *Lecture Notes in Physics 317*, ed. C. Signorini, et al. Berlin, Heidelberg: Springer-Verlag (1988), p. 93
31. Pass, C. N., et al., *Nucl. Phys.* A499: 173 (1989)
32. Guidry, M. W., et al., *Phys. Lett.* 163B: 79 (1985)
33. Gerl, J., et al., *Z. Phys.* A334: 195 (1989)
34. Macchiavelli, A. O., et al., *Nucl. Phys.* A432: 436 (1985)
35. de Boer, F. W. N., et al., *Z. Phys.* A325: 457 (1986)
36. Gammasphere, A National Gamma-ray Facility, The Proposal, ed. M. A. Deleplanque, R. M. Diamond, March 1988, Lawrence Berkeley Lab. Publ. 5202 (1988)
37. Jääskeläinen, M., et al., *Nucl. Instrum. Methods* 204: 385 (1983)
38. Rehm, K. E., et al., *Phys. Rev. Lett.* 51: 1426 (1983)
39. Rehm, K. E., See Ref. 30, p. 105
40. Juutinen, S., et al., *Phys. Lett.* 192B: 307 (1987)
41. Wu, C. Y., et al., *Phys. Lett.* 188B: 25 (1987)
42. Gerl, J., et al., *Phys. Rev.* C39: 1145 (1989)
43. Himmele, G., et al., *Nucl. Phys.* A404: 401 (1983)
44. Guidry, M. W., et al., *Nucl. Phys.* A361: 275 (1981)
45. Sapotta, K., et al., *Phys. Rev.* C31: 1297 (1985)
46. Elbek, B., Tjom, P. O., *Adv. Nucl. Phys.* 3: 259 (1969)
47. Künkel, R., von Oertzen, W., et al., *Z. Phys.* A336: 71 (1990)
48. Speer, J., von Oertzen, W., et al., *Annu. Rep.*, HMI-P. Hans-Meitner-Inst. In press (1989)
49. Hara, K., *Phys. Lett.* 35B: 198 (1971)
50. Dietrich, K., *Phys. Lett.* 32B: 428 (1970)
51. Landowne, S., Pollarolo, G., Dasso, C. H., *Nucl. Phys.* A486: 325 (1988)
52. Kleber, M., Schmidt, H., *Z. Phys.* 245: 68 (1971)
53. Gaudin, M., *Nucl. Phys.* A144: 191 (1970)
54. Stephens, F. S., In *Proc. Conf. High-Spin Nuclear Structure and Novel Nuclear Shapes*, April 1988. Argonne Natl. Lab., Ill. (1988), p. 139
55. Garrett, J. D., *Nucl. Phys.* A409: 259 (1983)

Annual Review of Nuclear and Particle Science
Volume 40, 1990

CONTENTS